University of Alberta

Synthesis, Kinematic Modeling, Parameter Identification and Control of a Rehabilitation Cable-Driven Robot

by

Omid Ghasemalizadeh

A thesis submitted to the Faculty of Graduate Studies and Research

in partial fulfillment of the requirements for the degree of

Master of Science

Department of Mechanical Engineering

Fall 2011

Edmonton, Alberta

Abstract

The proposed mechanism in this study is a multi-body cable driven robot. The robot has 6 DOF. The thesis first presents the required concepts and definitions. Then a solution to the kinematic synthesis problem is reviewed. This solution includes an algorithm that finds all the sets of design parameters that make the robot span a desired workspace. Also, an optimization procedure is proposed to find the best possible answer to the synthesis problem. Moreover, a geometrical approach is used to develop a parameter identification method. This task is very important since in practice the fabricated and assembled parts involve errors. More importantly, the robot is supposed to be configured before each performance and the new parameters need to be identified with acceptable accuracy.

Also, Impedance Control is investigated as a method of interest in rehabilitation. The simulation results on a simple shoulder rehabilitation cable robot are presented. The impedance Control makes the robot perform as a mass-spring-damper system. This property lets the patient deviate from the designated trajectory while guiding him towards the right path.

TABLE OF CONTENTS

LIST OF TABLES

LIST OF FIGURES

LIST OF SYMBOLS AND NOMENCLATURE

Abbreviations	Phrase / Definition
DOF	Degrees of Freedom / Number of coordinates that the position of the body can be described with
WCW	Wrench-Closure Workspace / a set of positions and orientations of the end-effector that can balance any external wrench.
FK	Forward Kinematics / Kinematic equations that give the position of end-effector based on variables of actuators
WFW	Wrench-Feasible Workspace / a set of positions and orientations (poses) of the end-effector where tensions of the cables remain in a specific range of values

Symbols	Definition
$\mathbf{n_{DoF}}$	Number of degrees of freedom of the system
$\mathbf{u}_\mathrm{i}$	A unit vector in the direction of the i^{th} cable pointing to the actuator
$\mathbf{A}$	Coefficient matrix of cable forces
$\mathbf{t}$	Vector of tensile forces in cables
$\mathbf{b}$	Vector of external forces and constraints
$\mathbf{s}_\mathrm{i}$	Vector of moment arm
$\mathbf{A}^\mathrm{t}$	Transpose of $\mathbf{A}$
$\mathbf{n}$	Null vector of $\mathbf{A}$
α	Arbitrary real value in the equation of cable forces
L	Lagrangian
T	Kinetic Energy
V	Potential Energy
q_i	i^{th} generalized coordinate
Q_i	i^{th} generalized force
Q_{i_c}	All the cable forces/moments
Q_{i_r}	All generalized force except cable
r_j	Position of the point where the cable is attached to the arm
$q_{i_{min}}$	Minimum values of the generalized coordinates
$q_{i_{max}}$	Maximum values of the generalized coordinates
h_i	Step size of the i^{th} generalized coordinate
q_{i_j}	The j^{th} grid point of i^{th} generalized coordinate
M_i	Space of possible positions of i^{th} actuator
g_{x_i}, g_{y_i}, g_{z_i}	x-coordinate, y-coordinate, and z-coordinate of i^{th} actuator respectively
θ_i	Rotation angle of i^{th} joint
$\mathbf{p}_j^i$	S vector with respect to frame j, expressed in frame i
$\mathbf{H}_b^a$	Transformation matrix that converts vector $\mathbf{p}_b^b$ to $\mathbf{p}_a^a$
R_{mn}	Transformation matrix of rotation with an angle of m occurred about the n axis
$Trans_{xl}$	Translation with magnitude of l along x direction
$\mathbf{P}_C$	Position of an Actuator
$\mathbf{P}_i$	Position of a fixed point for the parameter identification
l_i	Length of cable between fixed point and i^{th} known point

l_{s_i}, l_{t_i}	Straight and curved parts of cable respectively
φ	Angular position of the pulley about the direction of the cable
P_t	Tangent point located on the pulley
P_o	Center of the Pulley
F	The force applied by the actuator
f	External force the environment is applying on the system
m	Body's mass
x_d	Desired Trajectory
M_e, B_e, K_e	Desired inertia, damping and stiffness coefficients set by the user
$\bar{f}$	External force that the patient is applying ion the system
γ_i	The rotation angle of the i^{th} motor's spool
l_{0_i}	The initial length of the i^{th}cable
R	Radius of the motor's spool
q_d	Desired value of generalized coordinate
T_M	Motor's torque
T_C	Cable's torque
Δl	Displacement in cable's length
T_{O_i}	External forces that are applied by the user (patient)
$\bar{q_i}$	Deal value of i^{th} generalized variable

1 Introduction

1.1 Literature Review

Cable-driven is a term which refers to a division of mechanisms that are actuated by cables. Being light allows these kinds of systems to move with high speeds and accelerations. Moreover, having large workspaces and ease of reconfiguration with low cost makes them a good choice for a variety of applications. A few examples of cable-driven robots over the past two decades are NIST ROBOCRANE [1], FALCON [2], and DeltaBot [3].

These robots are considered as a subset of parallel mechanisms, although links are rigid in normal parallel robots. In cable robots, cables are counted as the links. Therefore, to preserve stability of a cable-driven mechanism, one has to make sure that all the cables remain in tension. A cable mechanism is called “tensionable” when a specific configuration of it is able to generate motion while all the cables remain taut. In order to ensure tensionability of a mechanism, the cable number should be at least one more than the degrees of freedom of the system [2].

The same statement can be made for tensionability of multi-body cable mechanisms [4]. In this case, the remaining problem is the distribution of cables among the bodies. For instance, connecting all the cables to one body might not preserve the tensionability. Thus, it is required to determine the regions in which the robot is tensionable.

Some work has been done on the analysis of tensionability in cable mechanisms. Verhoeven and Hiller [5] used the term “controllable workspace” as the tensionable region and defined it as “the set of poses in which robot can maintain equilibrium against all external wrenches”. Additionally, some other work contributed to the workspace analysis and determining the region of tensionability [6]. The same concept was used [7] for the optimal design of a 6 DOF parallel cable robot by considering workspace volume, accuracy of the robot for different configurations, and different poses of the end-effector.

Design and analysis of the workspace was done by Zi [8]. He studied a 3 DOF cable mechanism that is capable of applying high loads. The introduced mechanism drives a 3 DOF translational moving platform using 4 cables.

Gouttefarde [9] determined the Wrench-Closure Workplace (WCW) of a 6-DOF parallel mechanism. WCW is a set of positions and orientations of the “mobile platform for which the cables can balance any external wrench”. However, he only delineated the boundary for a “constant-orientation” workspace of the 6DOF mobile platform.

Chen [10] introduced a 3DOF cable-driven mechanism and used a methodology to optimize the parameters of its spherical joint. The robot was fixed to the global frame using a spherical joint and 4 cables were supposed to drive the moving platform. Chen also found the relationship between the cable forces and the pose of the end-effector.

Hassan [11] conducted a study on the analysis of the kinematics, workspace, and stiffness of cable robot manipulators. The robot was a 2DOF planar cable mechanism driven by eight cables with applications in warehousing. The boundaries of the workspace were derived analytically and the stiffness of the moving platform was investigated in order to maximize the lowest natural frequency.

Alikhani [12] presented an analysis of a spatial three DOF cable-driven robot which eliminates the rotational motion, “leaving the moving platform with three translational motions.” He found the geometrical description of the workspace boundary. He proposed a set of conditions on the geometry of the mechanism to form the workspace as a well-defined convex polyhedron. The same author [13] later designed the proposed mechanism. He used the geometry approach for synthesis of the robot, such that the end-effector is able to apply the desired moments and forces. The shape of the end-effector was a polyhedron. He also presented a fabricated prototype of the robot while considering the limitations of manufacturing.

Oftadeh [14] investigated the Forward Kinematics (FK) of a planar cable-driven mechanism compared to conventional rigid-link robots. He used the tension forces of cables as “extra sensory data” to propose a simplified analytical solution of FK. He claimed that his method “provides the sufficient performance” and “significantly reduces the process time compared to a similar method.”

Du [15] studied the forward kinematics of a large-span cable mechanism which has applications in radio telescope systems. He assumed that the end-effector moves slowly and that the dynamic effects are negligible. He also considered the cable sag effect to develop the Jacobian matrix. Furthermore, he presented numerical examples of his method to verify its accuracy.

Pham [16] analyzed the workspace of a fully restrained robot by introducing Tension Factor (TF). TF reflects the distribution of tension forces amongst all the cables and can be “an appropriate measure to evaluate the quality of tension restraint” for cable-driven robots. Later, Zhang [17] analyzed the WCW of a 6DOF cable-robot driven by 8 cables and showed a relation between the WCW and the dimension of the robot.

Lim, W.B. [18] introduced “a sufficient and necessary tension-closure condition.” He proved that his method is sufficiently general to ensure the tensionability of a cable-driven mechanism.

He then proposed an algorithm which is “computationally efficient” for pose analysis of a cable mechanism. The algorithm only needs to resolve a set of “deterministic linear equations.”

Hernandez-Martinez [19] introduced a measuring cable-driven robot called Milli-Cassino Tracking System (Milli-CaTraSys). He proposed an error estimation procedure to determine the impact of the error effect on the position and orientation of the end-effector. Moreover, he compared the results of simulation and the experimental tests “to show the feasibility and practical efficiency of a Milli-CaTraSys prototype”.

Another topic of workspace analysis which has become of interest to researchers in recent years is the Wrench Feasible Workspace analysis (WFW) [20]. The WFW of a cable robot is a set of positions and orientations (poses) of the end-effector where tensions of the cables remain in a specific range of values. The difference between WFW and WCW (Wrench Closure Workspace) is in the limitation on the cable forces. In WCW there is no limit on the tensile force and the only criteria is to have all the cables taut in the workspace. In other words, a WCW is a set of poses where the cables have non-negative tension forces.

Gouttefarde [21] gave a review of three useful characterizations of the force-closure approach. The force-closure workspace cable robot can generate any wrench on the end-effector by pulling the cables. He introduced 7 theorems of the mentioned characterizations. He used linear algebra to derive some of the proofs and proved the others using fundamental properties of polyhedral cones.

Loloei [22] analyzed the workspace of cable driven robot based on the “worst external wrench” approach. She proposed a new method to verify WFW which is applicable to “to any cable manipulators with any redundant cables as long as the Jacobian matrix is full rank.” She formulated the WFW in linear matrix inequalities.

Castelli [23] analyzed the kinematics of a 3 DOf cable-robot. The robot had 4 actuators and 8 cables. The cables were arranged in pairs with identical lengths. The purpose of his study was to “constrain the moving platform to keep a constant orientation with respect to the fixed frame.” He also simulated the robot numerically to investigate the kinetostatics and dynamics of the robot for large-scale applications.

Bouchard [24] introduced a new general and non-iterative method for the determination of the ability of a cable robot to generate a “given set of wrenches in a given pose” in a WFW. The cable robot has d DOF ($2 \leq d \leq 6$). His method is applicable to under-constrained and fully-constrained cable mechanisms.

Moreover, Rezazadeh [25] presented an analytical approach to the problem and set criteria of tensionability for multi-body cable mechanisms. He showed that using Lagrange’s method to

develop equilibrium equations of a multi-body cable driven mechanism makes the problem easier when it comes to the number of equations. For instance, a spatial 2-body cable robot that has 3 degrees of freedom will lead to 12 Newtonian equilibrium equations. However, Lagrange's method results in 3 equations which are less complicated and easier to analyze compared to a Newton-Euler formulation.

Synthesis of a cable robot is another topic in this field. Determination of the parameters of a mechanism to make it tensionable in a given workspace is found in several works. In 2005 Fattah [26] focused on the design of cable-driven robots. He first introduced a method to analyze the workspace of a robot. Then he explained how to obtain a region that is reachable by a fixed point on the solid body and named it as its workspace. He introduced a method which determines a range of parameters to satisfy a set of desired conditions. According to his method, the user should grid a range of parameters and for each grid-point the workspace would be determined using workspace analysis introduced in his study. At the end, each set of parameters which produces the closest workspace to the ideal one would be chosen by the user.

Another study in 2005 was conducted by Merlet [27]. He introduced a new mathematical method to solve a set of equations and inequalities and named it Interval Analysis. This method evaluates a range of variables in the equations and inequalities and returns one of the following three results:

1. None of the values in the range of variables satisfies the criterion.
2. All the conditions hold for all of the points.
3. Neither!

In Case (1) the whole range of variables will be removed, Case (2) proves that this range of variables satisfies the conditions, and the most important case is the last one, which leads to a bisection. This procedure continues and fillls all the boxes that have been approved or bisected by the procedure until the widths of all the boxes that have to be bisected become less than the error value, so they would be removed. At the end there will be some boxes remaining in the list that have been approved by the procedure. The final answer is some ranges of variables which are the solutions of equations and equalities.

In 2008 Goutterfarde, M. [28] used Interval Analysis efficiently and applied it to the design of a simple cable-driven robot. The planar robot was attached to four cables and it was assumed to have a rectangular shape. The length and width of the moving platform were taken as design parameters. Furthermore, he planned to gain the appropriate workspace with desired ranges of tensile force in cables and external wrenches on the moving plate. Using Interval Analysis, he solved the design problem and obtained a set of parameters that satisfied the conditions.

Xu [29] investigated the design and workspace optimization of a 6 DOF moving platform driven by 6 cables. He optimized the workspace of the moving platform based on the Jacobian matrix and shape of the moving platform.

Zanotto [30] introduced a set of indices that can be used for design optimization and performance analysis of the cable robots. He carried out a comparison of three cable robots on the kinematics and dynamics and showed the functionality of the introduced indices. The indices were “Power Dissipation Index”, “Dexterity Index”, and “Inertial Isotropy Index”.

Yao [31] designed and optimized a 4-cable-driven mechanism to meet the requirements in terms of cable tension and end-effector stiffness. He took the cable stiffness into account when deriving the equilibrium equations. To obtain the end-effector stiffness, he presented a practical stiffness analysis method.

Juhui [32] designed a 4-cable-driven robot for rehabilitation. The robot consists of 4 cables and a rigid body which is smoothly fabricated for safety of the patient. He simulated the operation of the robot using MATLAB and showed that the presented robot is operable.

1.2 Problem Statement

The aim of this study is to synthesize and control a cable-driven rehabilitation mechanism. The mechanism is supposed to learn a motion from the therapist and then repeat it a specific number of times. Physical therapy as a field of rehabilitation medicine requires complex motions, which in turn demand skilled personnel, complex machines, a complex robot, or several cooperating robots. Thus, we require a mechanism which is able to do a motion with even more than 6 degrees of freedom. Moreover, we desire a multi-functional robot which is not specifically designed for one limb. Even for a specific limb, there would be different sizes for different patients. Therefore, a reconfigurable robot is required so that the therapist can easily switch to an appropriate configuration. Furthermore, cost-effectiveness and simplicity are always concerns in the design and synthesis of a mechanism.

Eventually, a mechanism which is actuated by some cables was chosen for the following reasons:

- A cable-driven mechanism can be easily reconfigured simply by changing the position actuators.
- Using a cable mechanism, the therapist is able to teach complex motions, which are desired as previously mentioned. By using at least one more motor than the number of degrees of freedom, the mechanism can do the desired task.

- Since a cable-driven mechanism has cables instead of rigid links, the energy needed for each motion is much lower than conventional rigid-link robots.
- The cost of fabrication of rigid links is much higher than using cables.
- The kinetic energy that is stored in the inertia of the rigid links is potentially harmful to the patient.

The cable robot introduced in this chapter and used in this research is a multi-body mechanism with a maximum of 8 actuators, cables, a frame and a brace that the patient wears. The hardware of the robot was 80% built when this thesis started. During the course of the research, the remaining components were fabricated and installed.

Figure below shows the schematic view of the studied cable robot.

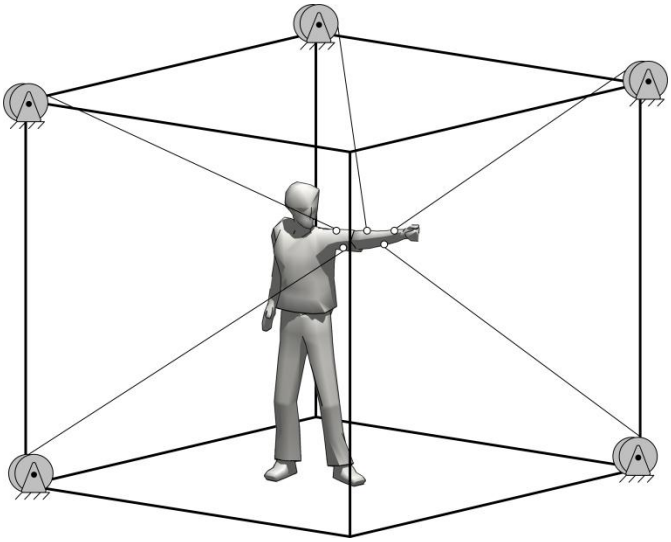

Figure 1-1 – Schematic view of the robot

As shown in the above figure, the core concept of the proposed robot is a cubic frame which was fabricated and the actuators were installed on the frame. Thus, the actuators can easily be fixed onto every point of the frame. The patient is placed in the frame wearing a brace, and the cables are connected to points on the brace. The actuators apply tensile forces on the cables and the cables drive the patient's limbs according to a desired trajectory.

In this research, synthesis, parameter identification, and control of such a robot were studied. Each chapter will be deals with one of these subjects. This study will not address the learning of a motion from the therapist; rather the goal of the control chapter is to track a given trajectory in a way that is comfortable and safe for the patient.

The synthesis chapter will go through the concepts and definitions of tensionability and the criteria for the tensionability of multi-body cable-driven robots. Then, an algorithm that

synthesizes a multi-body cable-driven mechanism for a desired workspace will be introduced. Also, an approach for optimizing the performance of a cable-driven mechanism will be addressed. The last part of the chapter will verify the presented material with a case study.

The next chapter considers the identification of the parameters of the mechanism of interest. Since the actual values of the parameters are not exactly the same as the resultant values of the synthesis, it is necessary to find the actual values of the parameters. The mathematics and geometry of the mechanism will be presented. At the end of this chapter, the estimation introduced method will be verified via a known and accurate method.

The control chapter of this study addresses the basic concept of impedance control. An implementation of impedance control on a multi-body cable robot is described; and a shoulder rehabilitation mechanism will be simulated using MATLAB SimuLink as a case. The thesis concludes with a summary of contributions and recommendations for future work.

2 Kinematics Synthesis

The goal of this chapter is to synthesize the cable-driven mechanism introduced in the last chapter for physical therapy applications. The components of the mechanism are introduced and the procedure of synthesis is explained in the following section. This chapter will go through the details of an algorithm that returns a specific configuration of a robot such that it operates in a desired workspace. The algorithm takes the workspace and all possible configurations and calculates a set of parameters as the final configuration.

It should be noted that not all the parameters are meant to be obtained from the synthesis procedure, due to the nature of the introduced mechanism. Some parameters remain constant throughout the design process. However, the other parameters (positions of actuators) satisfy the goal of the synthesis, which is to find a configuration which allows the robot to provide the given workspace with acceptable accuracy.

The mechanism is designed for the rehabilitation of an arm consisting of shoulder and elbow. The arm model is presented and the fabricated model is shown. In addition, there is a frame upon which the actuators are installed.

After the mechanism introduction, some concepts and definitions for cable robots are discussed and some equations are noted to develop the synthesis criteria. It should be mentioned that the synthesis criteria which is used in this study is taken from a published study in the field of multi-body cable-driven robots [25].

According to the derived equations and mentioned criteria an algorithm was developed and is introduced in this study. Furthermore, a method of optimization is presented which uses a cost function to optimize the design.

At the end of this chapter, the algorithm is implemented on the introduced mechanism. Moreover, a case study is considered for this chapter: a practical mechanism which has been fabricated and assembled by following the directions of this study. The final design specifications are also presented.

2.1 The Robotic Setup

The robotic setup of this study consists of a model arm, 5 actuators, a frame that the actuators have been installed on, and 5 cables that were attached to the arm at one end and wound around the actuator spools at the other end.

The model of the arm that has been considered for this study is shown below.

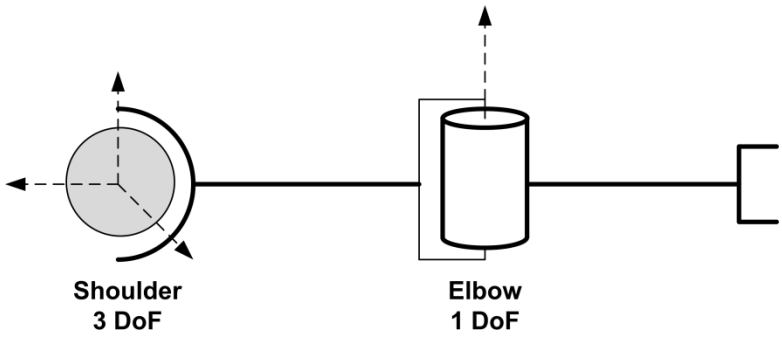

Figure 2-1 – Model of the arm

As is shown in Figure 2-1, the arm has 4 degrees of freedom, 3 of them belonging to the shoulder and the other one to the elbow. The arrows show the direction of rotation for each joint. Each body of the arm is a cylinder with a radius of 2.54 cm.

A fabricated model of the arm is shown in Figure 2-2.

Figure 2-2 – Fabricated model of arm

The arm is fixed to a beam in the middle of the frame. Dimensions and specifications of the arm will be explained in the case study section.

Figure 2-3 shows all the components together in one figure. The arm is fixed through the spherical joint in the reference frame. The coordinate system is depicted as well. It should be mentioned that the center point of the spherical joint is assumed to be the origin of the main coordinate frame. Therefore, all the coordinates in the global frame should be noted with respect to this point. It will be used frequently in the parameter identification in chapter 3.

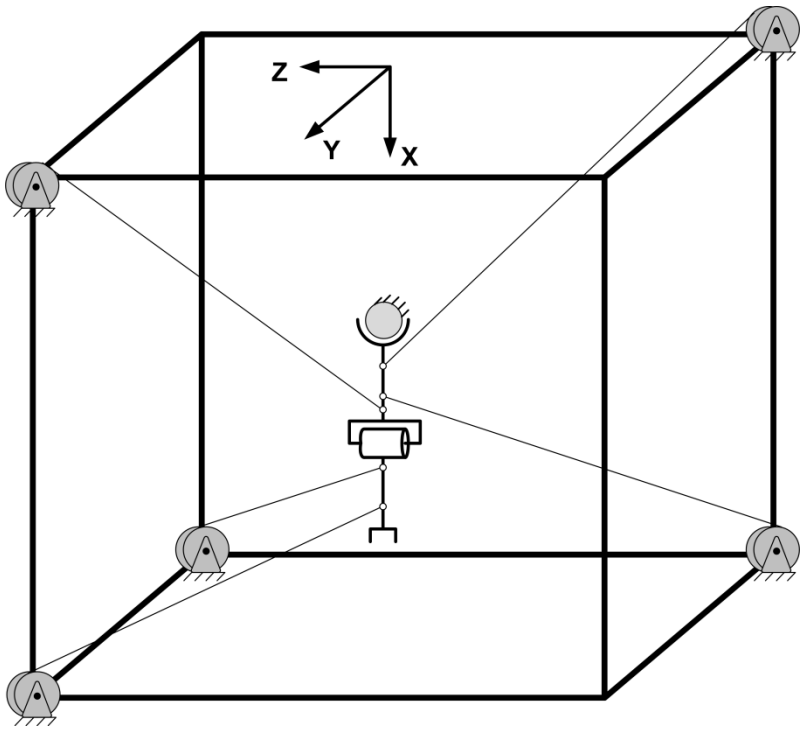

Figure 2-3 – Schematic view of the studied mechanism

The actuators apply tensile force on the cables and consequently the arm either stays in its position or moves around. The very first concern is how to determine the parameters of the system. There are two types of parameters and each has to be investigated individually. First, there are parameters for arm specifications such as length of each part and position of points that the cables are attached to. The other parameters are the positions of actuators. Since the patient is supposed to wear a brace and the cables are connected to particular points on it, there are not many choices when deciding the position of such parameters. As a result, in this study the first types of parameters are assumed to be known and constant. Based on this assumption the synthesis would be mainly about finding the exact position of the actuators. Therefore, the term “Design Parameters” refers to the second type, the position of the actuators.

Figure 2-4 shows the fabricated frame.

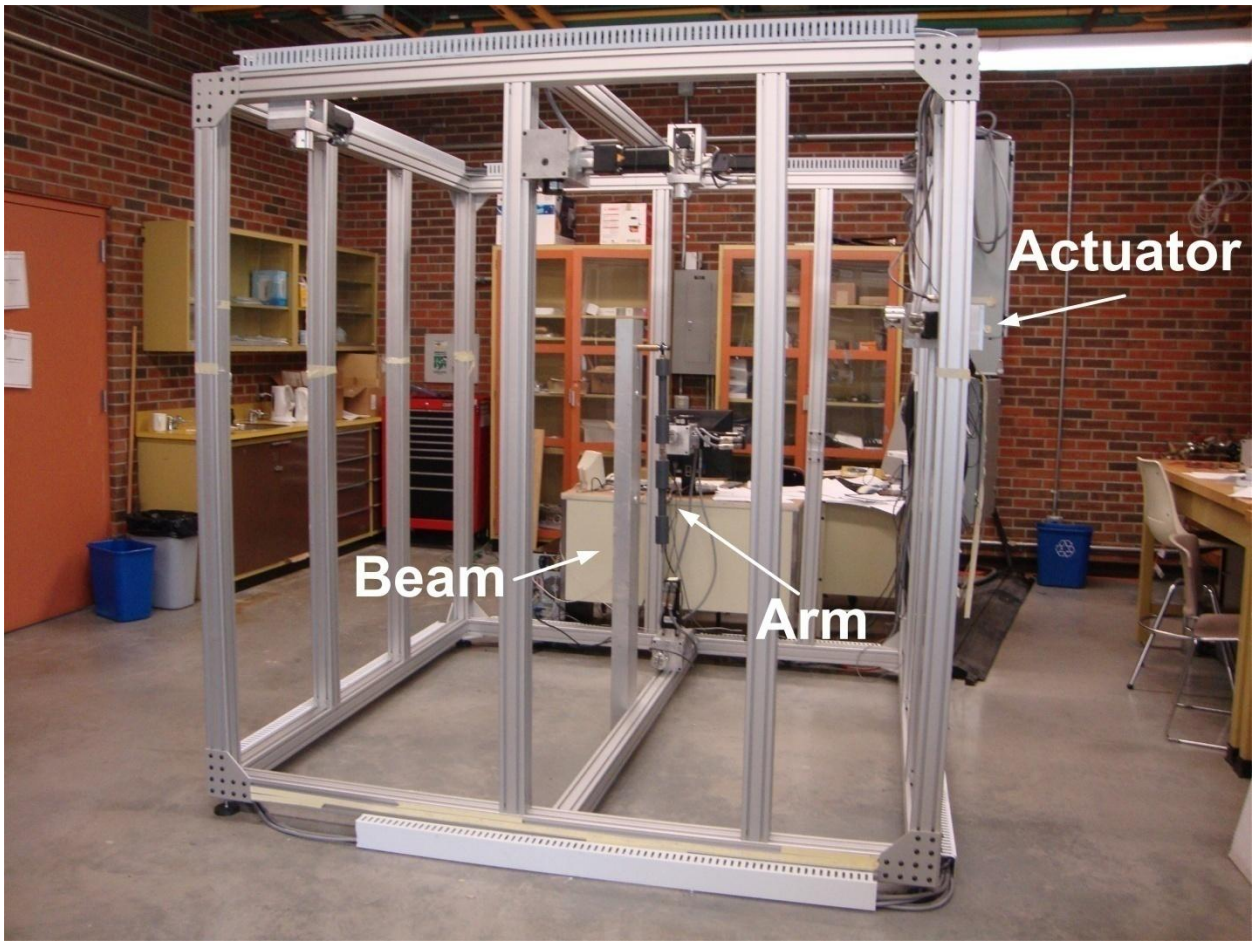

Figure 2-4 – Fabricated mechanism and actuators

The whole mechanism is a multi-body cable-driven system. In this study, the shoulder and elbow are modeled with spherical and revolute joints, respectively. Therefore, the considered model has 4 degrees of freedom. According to [2], at least $n_{DoF} + 1$ actuators should be attached to an n_{DoF} degrees of freedom cable-driven mechanism to provide tensionability; that is any motion on the arm can be generated while maintaining tensile force in all cables. Since the arm has 4 DoF, a minimum of 5 actuated cables are needed to fulfill the tensionability requirement. It should be mentioned that the definition and concept of tensionability will be discussed in the next section. To calculate the number of cables for each link, the same criteria can be used. The first link has 6 DoF, as a rigid body, and is over-constrained because of the two mentioned joints next to it. The spherical joint has 3 translational constraints and the revolute join provides 2 rotational relative constraints as well as 3 translational relative constraints. Therefore, it would not need any cable essentially, but the other link has only 5 constraints (because of the revolute joint) which means at least 2 cables should be attached to fully constrain it. The table below briefly shows all the above statements.

Table 2-1 – Link and Minimum Number of Cables

Name	DoF	Constraints	Min. Number of Cables
Link 1	6	Over-Constrained	0
Link 2	6	5	2
Whole Mechanism	12	8	5

2.2 Tensionability and Design

As was mentioned at the beginning of this chapter, the goal is to determine the parameters of the system in a way that the given workspace is covered. In other words, designing a robot which spans a given workspace is desired. The algorithm which is proposed in this section includes three main parts; and, by following them, one would obtain a desired set of parameters. Before going through the details of those three parts, it is necessary to describe the problem in engineering terms.

Like every other engineering design problem, we have a variety of choices and requirements. The problem is how to find one design amongst many possibilities to produce a robot that meets the requirements.

The option is a range of design parameters and the requirement is the workspace that has to be covered. The answer would be a set of values for the design parameters that corresponds to a unique cable-driven robot. The obtained robot is supposed to be working within the given workspace. Therefore, the mentioned code would have two inputs; range of design parameters and desired workspace. Moreover, the output would be a set of design parameters. Figure 2-5 illustrates how the design optimization code is supposed to work.

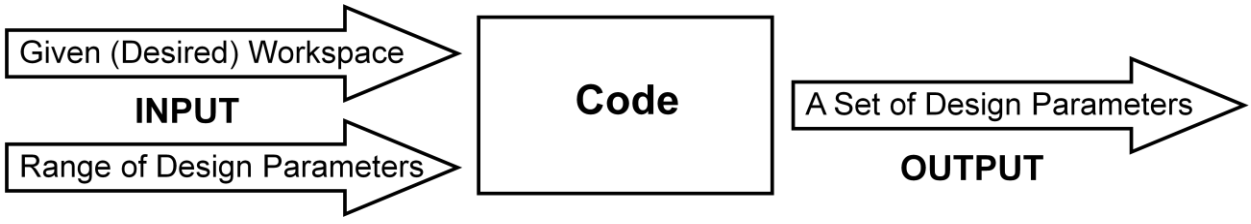

Figure 2-5 - Scheme of the synthesis problem

Before dealing with the synthesis problem some definitions and concepts need to be discussed.

Tensionability is the most important subject in cable-driven robotics because in these systems, cables can only afford tensile force. In other words, compression in cables leads to buckling. For

example, in the figure below, it is impossible to move the grey point in any desired direction - without existence of a third motor.

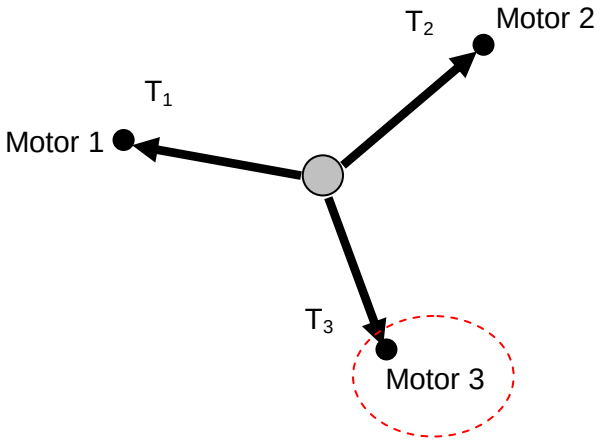

Figure 2-6 – A system with three cables

The above figure shows that for a 2 DoF motion in the plane, three cables are needed. From the literature [2] it is known that for an n_{DoF}system, there should be $n_{DoF} + 1$cables (actuators).

In order to investigate the tensionability of cable-driven mechanisms mathematically, we need an analytical description of this property. This description can be found in the equilibrium equations of the system.

Figure 2-7 shows the schematics of a rigid body cable-driven mechanism of m cables in general.

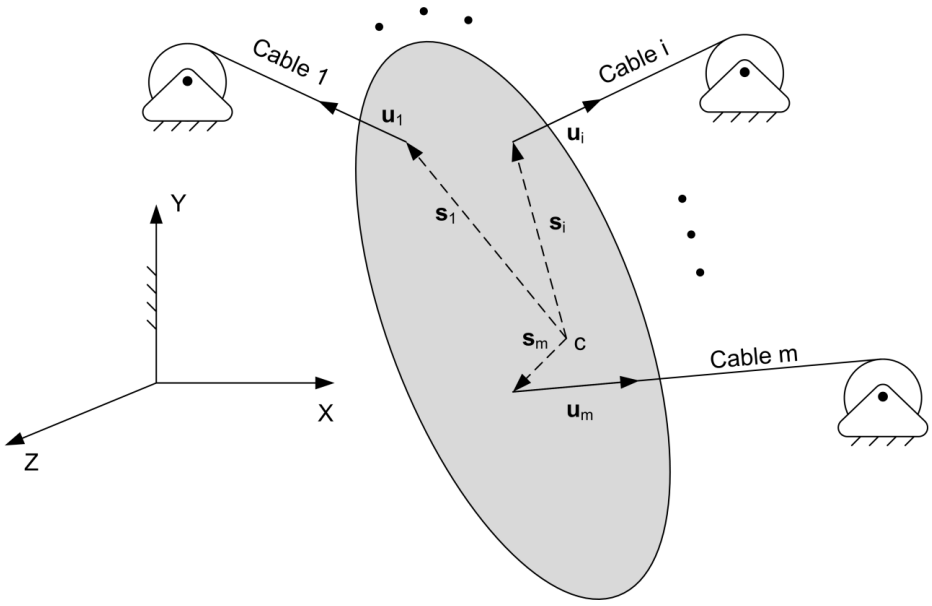

Figure 2-7 – Schematics of a rigid body cable-driven mechanism

For the above system one can write Newton's equilibrium equations as

$$\mathbf{At} = \mathbf{b} \tag{2-1}$$

where $\mathbf{A}$ is a n_{DoF}-by-m matrix, $\mathbf{t}$ is a vector of tensile forces in cables and $\mathbf{b}$ is the resultant vector of external forces and constraints:

$$\mathbf{A}_{n_{DoF}\times m} = \begin{bmatrix} \mathbf{u}_1 & \mathbf{u}_2 & \dots & \mathbf{u}_\mathrm{m} \\ \mathbf{s}_1 \times \mathbf{u}_1 & \mathbf{s}_2 \times \mathbf{u}_2 & \dots & \mathbf{s}_\mathrm{m} \times \mathbf{u}_\mathrm{m} \end{bmatrix} \tag{2-2}$$

$$\mathbf{t}_{\mathrm{m}\times 1} = [\mathrm{t}_1 \quad \mathrm{t}_2 \quad \dots \quad \mathrm{t}_\mathrm{m}]' \tag{2-3}$$

where $\mathbf{u}_\mathrm{i}$ is a unit vector in the direction of the i^{th} cable pointing to the actuator, $\mathbf{s}_\mathrm{i}$ is the corresponding moment arm, and n_{DoF} is 3 for planar and 6 for spatial systems in single-body cable-driven mechanisms.

In order for equation (2-1) to have at least one solution for an arbitrary loading, matrix $\mathbf{A}$ should be full-rank. In other words, m should be equal or greater than n_{DoF}.

From linear algebra, if matrix A is full-row rank, the solution of equation (2-1) is:

$$\mathbf{t} = (\mathbf{A}^\mathrm{t}\mathbf{A})^{-1}\mathbf{A}^\mathrm{t}\mathbf{b} + \alpha\mathbf{n} \tag{2-4}$$

where $\mathbf{A}^\mathrm{t}$ is the transpose of $\mathbf{A}$, $\mathbf{n}$ is the null vector of $\mathbf{A}$ and α is an arbitrary real value. If $\mathbf{A}$ is a square full-rank matrix, then the solution of $\mathbf{t}$ is unique and depends on $\mathbf{b}$. Therefore, there is no guarantee that all the components of $\mathbf{t}$ are positive, i.e. have tension in all cables. It can be concluded that we need at least $n_{DoF} + 1$ cables to ensure all the cables are in tension.

In order have all components of $\mathbf{t}$ with positive signs, we need to ensure all components of $\mathbf{n}$ are of the same sign. If this condition is met then one can make the signs of all elements of $\mathbf{t}$ positive by assuming a sufficiently large value for α with appropriate signs. Therefore, the second term of the right-hand side becomes a vector with large enough positive components and that cancels the effect of the first term.

The above statements can be summarized as follows: for a cable-driven mechanism to be tensionable,

1. $\mathbf{A}$ should be full-rank (and)
2. Null vector of $\mathbf{A}$ should have all the components of the same sign.

Therefore, the two mentioned criteria should hold to have a cable-driven robot tensionable in a specific position since matrix $\mathbf{A}$ depends on the position of the rigid body. At first, the coefficients matrix should have a rank of n_{DoF} (which is the number of rows) and second, the null vector of this matrix has to have nonzero and same sign components.

If the cable-driven mechanism is not a single rigid body and consists of several links, the internal forces at the joints will show up in the equilibrium equations. Consequently, the equations become more complicated and the size of matrix $\mathbf{A}$ would increase. For instance, for a 4 link spatial mechanism, matrix $\mathbf{A}$ has 24 rows and at least 25 columns. The large size of the matrix is due to the existence of the internal unknown forces. To address this problem, another method of formulating the equilibrium should be used.

For serial multi-body mechanisms, using Lagrange's approach and generalized force notation reduces the complexity of the equilibrium equation by eliminating the internal forces corresponding to interaction of bodies.

In Lagrange's [33] method, a set of coordinates called generalized coordinates are defined such that the Lagrangian equation (2-5) can be analytically expressed in terms of them. If the number of such coordinate variables is equal to the number of degrees of freedom, they are said to form a minimum coordinate set and the dynamics of the system can be expressed only by n_{DoF}differential equations in Lagrange's equation:

$$L = T - V \tag{2-5}$$

$$\frac{d}{dt}\left(\frac{\partial L}{\partial \dot{q}_i}\right) - \frac{\partial L}{\partial q_i} = Q_i \ (i = 1, \dots, n_{DoF}) \tag{2-6}$$

where L, T, and V are the Lagrangian, kinetic energy, and potential energy, respectively. Also, q_i and Q_i are the i^{th} generalized coordinate and force.

In the case of a cable mechanism, the right-hand side of Lagrange's equation can be divided into two parts as shown below:

$$Q_i = Q_{i_c} + Q_{i_r} \tag{2-7}$$

where Q_{i_c} represents all the cable forces/moments and Q_{i_r}expresses all the other generalized forces/moments. By taking Q_{i_r} to the left-hand side of equation (2-7) and substituting Q_i from equation (2-6), one can rewrite equation (2-7) as shown below.

$$\frac{d}{dt}\left(\frac{\partial L}{\partial \dot{q}_i}\right) - \frac{\partial L}{\partial q_i} - Q_{i_r} = Q_{i_c} \tag{2-8}$$

According to Lagrange's method, one can write Q_{i_c} in terms of the cables forces.

$$Q_{i_c} = \sum_{j=1}^{m}\left(t_j \mathbf{u}_j . \left(\frac{\partial \mathbf{r}_j}{\partial q_i}\right)\right) = \left[\mathbf{u}_1 . \left(\frac{\partial \mathbf{r}_1}{\partial q_i}\right) \quad \dots \quad \mathbf{u}_m . \left(\frac{\partial \mathbf{r}_m}{\partial q_i}\right)\right] \begin{bmatrix} t_1 \\ \vdots \\ t_m \end{bmatrix} \tag{2-9}$$

where $\mathbf{u}_j$ is a unit vector that lies on the direction of j^{th} cable and points to the fixed end of it, and $\mathbf{r}_j$ is the position where the cable is attached to the arm.

Therefore, for all the generalized coordinates the equation (2-9) can be written as shown below:

$$\begin{bmatrix} Q_{1_c} \\ \vdots \\ Q_{n_{DoF_c}} \end{bmatrix} = \begin{bmatrix} \mathbf{u}_1.\left(\frac{\partial \mathbf{r}_1}{\partial q_1}\right) & \dots & \mathbf{u}_m.\left(\frac{\partial \mathbf{r}_m}{\partial q_1}\right) \\ \vdots & \ddots & \vdots \\ \mathbf{u}_1.\left(\frac{\partial \mathbf{r}_1}{\partial q_{n_{DoF}}}\right) & \dots & u_m.\left(\frac{\partial \mathbf{r}_m}{\partial q_{n_{DoF}}}\right) \end{bmatrix} \begin{bmatrix} t_1 \\ \vdots \\ t_m \end{bmatrix} \tag{2-10}$$

Again, one can write the equations of the system in the form of equation (2-1) but this time the number of rows for matrix $\mathbf{A}$ equals the number of degrees of freedom. Therefore, the solution for that equation would be the in form of equations (2-4) if the matrix $\mathbf{A}$ is full-row rank. It is obvious that the method of formulating the equilibrium does not make any difference in the conditions of tensionability, although it may make it easier to verify. Now equation (2-10) can be written in the following way:

$$\mathbf{A}_L \boldsymbol{\tau}_L = \mathbf{b}_L \tag{2-11}$$

Where $\boldsymbol{\tau}_L$ is a vector of tensile forces and $\mathbf{A}_L$ is the coefficient matrix of (n_{DoF})-by-(at least $n_{DoF} + 1$). Also, $\mathbf{b}_L$ is a vector consisting of the left-hand side of equation (2-8).

In fact, Equation (2-11) is the matrix form of equilibrium equations of the system. If a system has n_{DoF} degrees of freedom and m cables ($m > n$) then the coefficient matrix is as follows:

$$\mathbf{A}_{L_{n_{DoF} \times m}} = \begin{bmatrix} u_1.\left(\frac{\partial r_1}{\partial q_1}\right) & \cdots & u_m.\left(\frac{\partial r_m}{\partial q_1}\right) \\ \vdots & \ddots & \vdots \\ u_1.\left(\frac{\partial r_1}{\partial q_{n_{DoF}}}\right) & \cdots & u_m.\left(\frac{\partial r_m}{\partial q_{n_{DoF}}}\right) \end{bmatrix} \tag{2-12}$$

Now, one can easily find out if a cable mechanism is tensionable in a specific position simply by evaluating matrix $\mathbf{A}_L$. Also, the mentioned matrix consists of u_i's, r_i's, and q_i's. Furthermore, both u_i and r_i are in terms of some parameters (lengths) and q_i (generalized coordinate). In other words, $\mathbf{A}_L$ is in terms of q_i's and that means the tensionability only depends on the position of a cable mechanism. The same criteria are used for matrix $\mathbf{A}_L$, to check the tensionability of a mechanism:

1. $\mathbf{A}_L$ should be full-rank (and)
2. Null vector of $\mathbf{A}_L$ should have all components of the same sign.

Note that due to elimination of internal forces, the size of matrix $\mathbf{A}_L$ has reduced significantly. For instance, in a 4 link serial spatial mechanism size of matrix $\mathbf{A}_L$ is 4 rows and at least 5 columns which makes the calculation easier than using Newton's method, which returns a matrix of 24 rows and at least 25 columns for the same mechanism.

2.3 Workspace Evaluation and Design Algorithm

Assume we have a desired work space and we want to see if a particular design of the robot is tensionable in each single point of that workspace. Assume that a workspace is given in the form of Cartesian coordinates and the task is checking tensionability of the robot in the desired region. Since the mentioned criteria could be only applied for a specific point, it is hardly possible to check the tensionability of a given workspace in analytical form.

One solution is to check the tensionability numerically. In order to do that, the first step is to grid the given space (region) and check each grid point with the tensionability criteria. It is obvious that accuracy of results depends on grid step size. For example, if the grid points are too far away from each other and a non-tensionable region exists between two grid points, then the result will not show any non-tensionability although the given workspace is not tensionable. Figure 2-8 illustrates how it may happen.

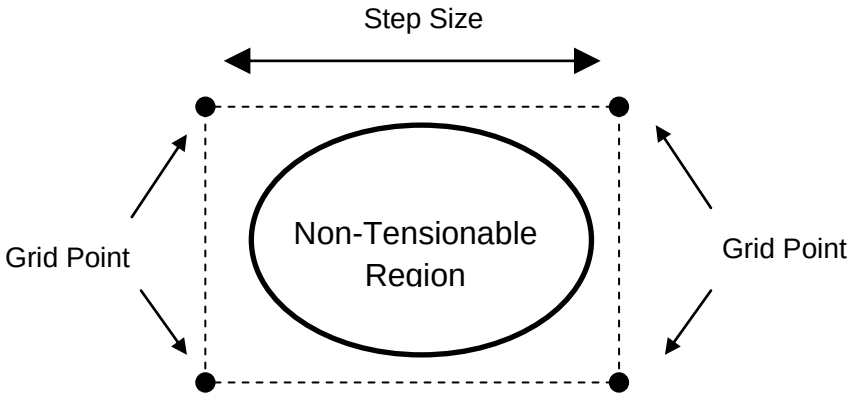

Figure 2-8 – Existence of non-tensionable region between grid points

As depicted in Figure 2-8, the non-tensionable area is located between the grid points; and by applying the tensionability criteria one would find the workspace tensionable.

The problem becomes even harder when the system has more than one body. It is hard to check the tensionability analytically because of nonlinear terms. Most of the time, the given workspace of a multi-body mechanism is described using a joint coordinate system. Therefore, checking the tensionability conditions for a given space of joint coordinates makes sense. One

can grid the joint coordinates space into a finite number of points and check the tensionability criterions for each grid point.

For example, consider the case shown in Figure 2-9. For the mentioned case, there are two joint variables (θ_1 and θ_2) and the given workspace is given in the space of those two. The figure below shows how the workspace, which lies in the space of the joint variables, can be reduced to a finite number of grid points.

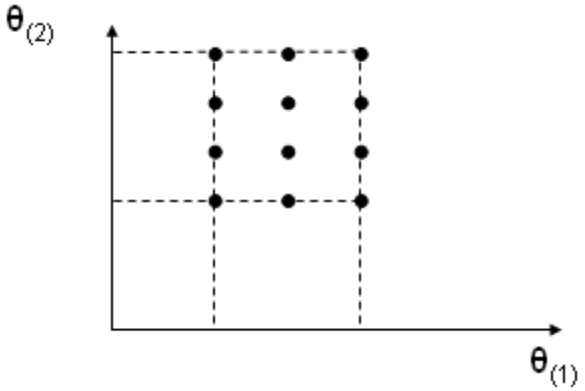

Figure 2-9 - Workspace that lies in space of joint variables

The method that is used in this study for evaluating a given workspace is explained in Figure 2-10.

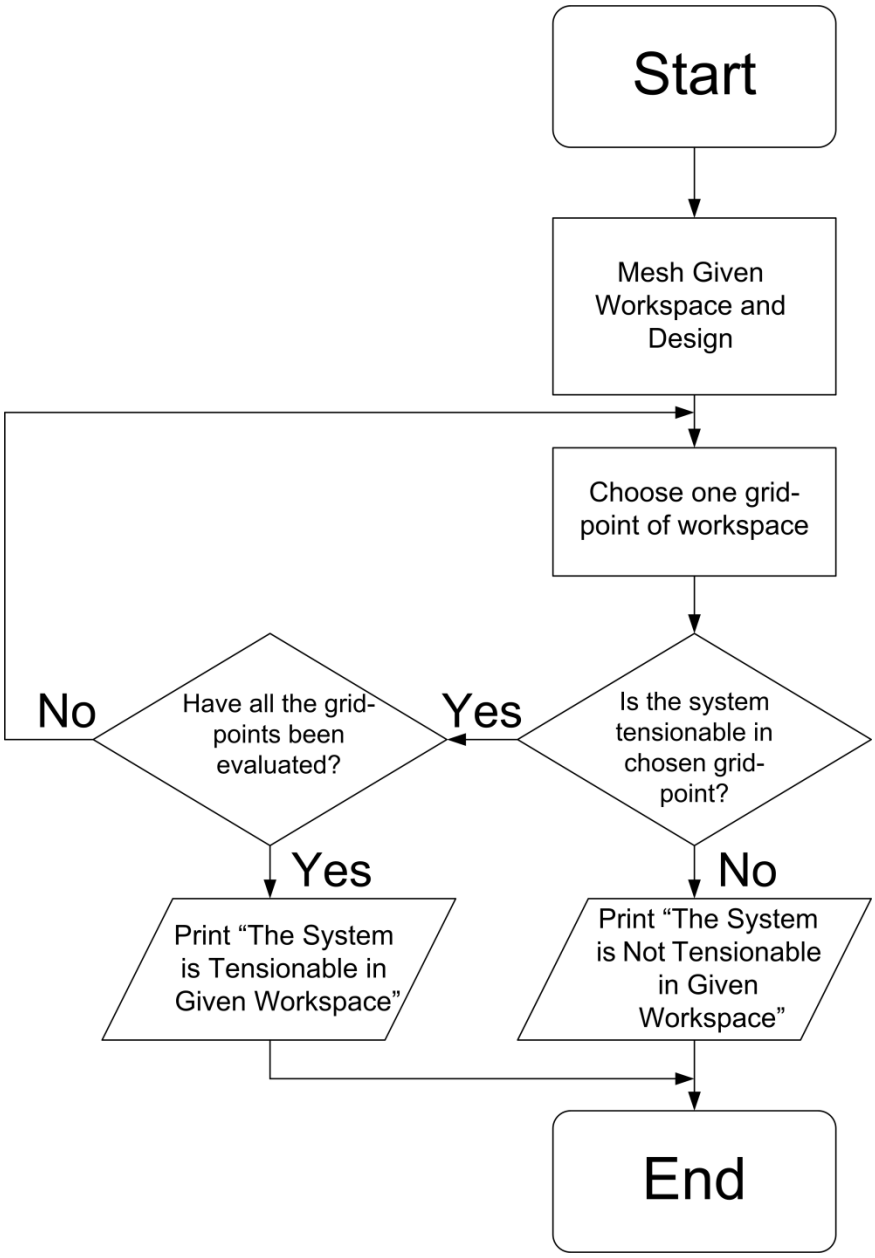

Figure 2-10 – Algorithm of evaluating a given workspace

As shown in figure above, the first step is to mesh the given workspace. The user specifies a step size for each coordinate variable and based on the value of the step sizes, the workspace will be meshed into a specific number of nodes. Assume that the workspace is given as below:

$$\{(q_1, \dots, q_{n_{DoF}}) | q_{1_{min}} < q_1 < q_{1_{max}}; \dots; q_{n_{DoF_{min}}} < q_{n_{DoF}} < q_{n_{DoF_{max}}}\}$$
$$\text{or} \qquad (2\text{-}13)$$
$$\left\{\left[q_{1_{min}}, q_{1_{max}}\right], \dots, \left[q_{n_{DoF_{min}}}, q_{n_{DoF_{max}}}\right]\right\}$$

where q_i's are the generalized coordinates (and also, joint variables). $q_{i_{min}}$'s and $q_{i_{max}}$'s are minimum and maximum values of the joint variables. Equation (2-13) says that the given workspace has n_{DoF} dimensions.

By assuming h_i as the step size of the i^{th} variable (q_i), the meshed version of a given work space can be described as shown below:

$$\left\{\left\{q_{1_{min}}, \dots, q_{1_j}, \dots, q_{1_{max}}\right\}, \dots, \left\{q_{i_{min}}, \dots, q_{i_j}, \dots, q_{i_{max}}\right\}, \dots, \left\{q_{n_{DoF_{min}}}, \dots, q_{n_{DoF_j}}, \dots, q_{n_{DoF_{max}}}\right\}\right\} \quad (2\text{-}14)$$

where the q_{i_j} is the j^{th} grid point of i^{th} variable and its value can be obtained using the following equation:

$$q_{i_{j+1}} = q_{i_j} + h_i \quad (2\text{-}15)$$

Equation (2-14) represents a finite space of n_{DoF} dimensions that has step-sizes of equal size for each dimension.

Having the workspace meshed, the algorithm picks the grid points one by one and in a specific order, while evaluating them using tensionability criteria. Once one grid-point fails in the evaluation, the algorithm returns the workspace as non-tensionable. If, and only if, all the grid points hold the criteria, then the given workspace is labeled as tensionable. This means that the mechanism can span the workspace and the accuracy of the result depends on the value of the step-size as previously mentioned. The stated process is shown in Figure 2-10.

By now, we know how to evaluate a desired workspace using the criteria, but the main problem is to develop an algorithm which synthesizes a mechanism that is tensionable in a desired workspace. Note that the term "synthesis" here means to find the position of actuators since the configurable parts of the cable mechanism are actuator positions

To do so, one can pick a feasible arbitrary configuration of actuators and check the tensionability of the mechanism in the desired workspace, using the method described in the previous section. In order to check all the possible configurations of the actuators for tensionability and find the best one, it would be better to define a space of the actuator positions, which is noted as "Design Parameters Space," and mesh that space using a preset step-size value. The dimension of the Design Parameters Space depends on the number of actuators and the type of mechanism. For instance, an n_{DoF} spatial mechanism has $3 \times$ at least $(n_{DoF} + 1)$ dimensions of Design Parameters Space, since each actuator has 3 coordinate parameters (x, y, and z). Again, the accuracy of the results would depend on the values of the step-sizes. Since the position of actuators are defined in the Cartesian coordinates the dimension of the Design Parameters Space is $3 \times (n_{DoF} + 1)$.

Each actuator's space can be described by the allowed ranges of its Cartesian coordinates as shown below.

$$M_i = \{[x_{i_{min}}, x_{i_{max}}], [y_{i_{min}}, y_{i_{max}}], [z_{i_{min}}, z_{i_{max}}]\} \tag{2-16}$$

M_i is space of possible positions of i^{th} actuator.

Having the Design Parameters Space and appropriate step-size, one can mesh it as was done for the workspace. Assuming that the step-size for the x-coordinate, y-coordinate, and z-coordinate of i^{th} actuator are g_{x_i}, g_{y_i}, and g_{z_i} respectively, each actuator's meshed space is shown below.

$$\acute{M}_i = \left\{\{x_{min}, \dots, x_j, \dots, x_{max}\}, \{y_{min}, \dots, y_j, \dots, y_{max}\}, \{z_{min}, \dots, z_j, \dots, z_{max}\}\right\} \tag{2-17}$$

where the values of x_j, y_j, and z_j can be obtained from the following equations.

$$\begin{aligned} x_{i_{j+1}} &= x_{i_j} + g_{x_i} \\ y_{i_{j+1}} &= y_{i_j} + g_{y_i} \\ z_{i_{j+1}} &= z_{i_j} + g_{x_i} \end{aligned} \tag{2-18}$$

Having all $\acute{M}_i$, one can simply write a larger space which is the meshed version of Design Parameters space. According to Equations (2-16), (2-17), and (2-18) the meshed Design Parameters Space can be described as shown below.

$$\{M_1, \dots, M_{n_{DoF+1}}\} \tag{2-19}$$

An algorithm was developed to let the user synthesize appropriate design parameters for a given workspace. The algorithm first meshes the given workspace as in equation (2-14) and Design Parameters Space based on equation (2-19). Then it picks a set of design parameters, based on a specific order, from the meshed space and evaluates the given workspace as was shown in Figure 2-10. If the workspace is tensionable for the set of design parameters, it will flag it as a solution to the synthesis problem; otherwise the algorithm ignores it. Regardless of whether the set of design parameters is flagged as a solution or not, the algorithm goes to the next cycle and does the same for all the grid points of the meshed Design Parameters Space. After the algorithm is done with all the grid points, it will print out all the flagged solutions, if there is any.

The figure below depicts the flowchart of synthesis algorithm.

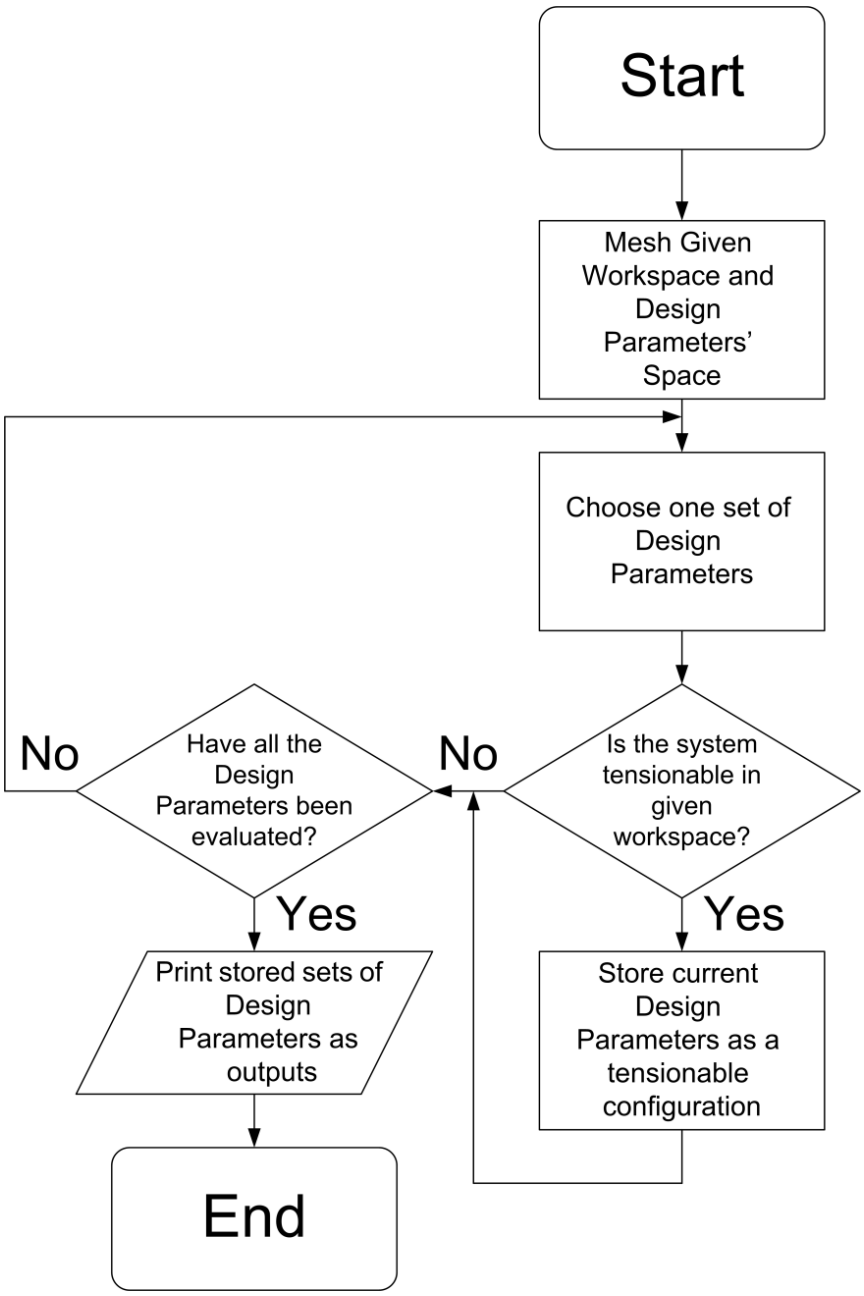

Figure 2-11 – Synthesis flowchart

2.4 Design Optimization

Now we have several solutions, each of which recommends a set of design parameters or in other words, a particular configuration for the mechanism. The problem is how to pick the best or the one that is most feasible to the user's need. In order to have the best solution, a criterion should be set and a cost function has to be introduced; the solution that has the minimum value of cost function would then be the final answer.

In this study, the solution that has the minimum variance of components of vector $\mathbf{n}$, according to equation (2-4), was chosen. In other words, the objective function is the variance of $\mathbf{n}$'s components. The reason is explained in the next paragraphs.

According to equation (2-1), the null vector of matrix $\mathbf{A}$, which is named as $\mathbf{n}$, is a part of solution of $\mathbf{t}$ for the same equation. Therefore, components of $\mathbf{n}$ represent the pattern of tensile forces in cables that are used to increase all cable force to positive values. Moreover, it is desired to have magnitudes of forces with low variance so the actuators' working condition will be close to each other.

Also, to obtain more accurate results, one can fine tune the selected solution of the last step. To do so, one can find the best set of obtained solutions by evaluating all of them using the mentioned criterion and then try to go in the opposite direction of the cost function's gradient. In other words, having the best obtained solution, one can likely find a better solution to the problem near to the resultant grid point, in the Design Parameter Space. The gradient of the cost function would guide us to a point in the space which has a smaller cost function than the grid point does. It should be noted that this method does not guarantee to achieve the optimal solution but it reduces the chance of being trapped in local minima points.

Figure 2-12 shows a two dimensional Design Parameter Space. The circles represent the grid points that are flagged as solutions and the dotted lines depict the direction of gradients. The red circle is the set of design parameters that has a minimum cost value amongst the others and the red line shows the gradient line that passes through it. It shows how the previously described method works.

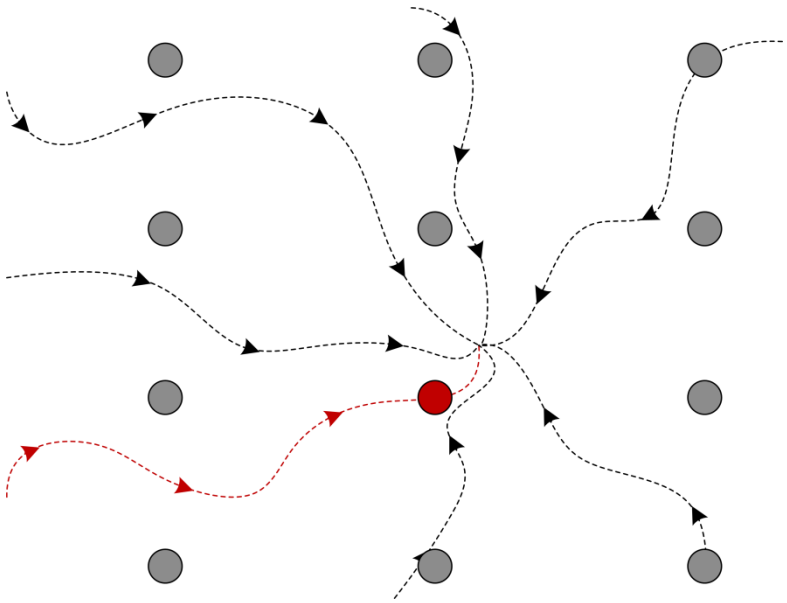

Figure 2-12 – Meshed Design Parameter Space of a simple mechanism

One may ask why the Design Parameter Space has been meshed since the gradient line would be enough to find the best solution. Theoretically, the answer is yes, but when it comes to practical cases, following the gradient lines based on a nonlinear cost function may cause the search to be trapped in a local minima. There are many points in the Design Parameter Space that the cost function has the minimum value compared with the points around it. In other words, the gradient approaches zero value at these points, but they do not have essentially the absolute minimum value of the cost function. The goal is to find the point that has the lowest value of cost function amongst all other points in the Design Parameter Space.

In this method, meshing and taking the best grid point, by evaluating all the grid points in objective function, gives a point that is close enough to the minimum point, which can be used as the initial point of the optimization process. Again, the accuracy of this method depends on value of step-size.

2.5 Implementation of Mentioned Synthesis Method on the Robot

By now, all the materials that are needed for the synthesis of the mechanism have been collected and developed. The next step is to implement those materials on the rehabilitation mechanism. According to the previous section the first step is to obtain matrix $\mathbf{A}_L$ based on equation (2-12).

However, one needs to determine the positions of the points on the arm that the cables are attached to. In other words, u_i's and r_i's are needed in terms of q_i's. The model of the arm shown in Figure 2-1 is expanded and shown in the figure below.

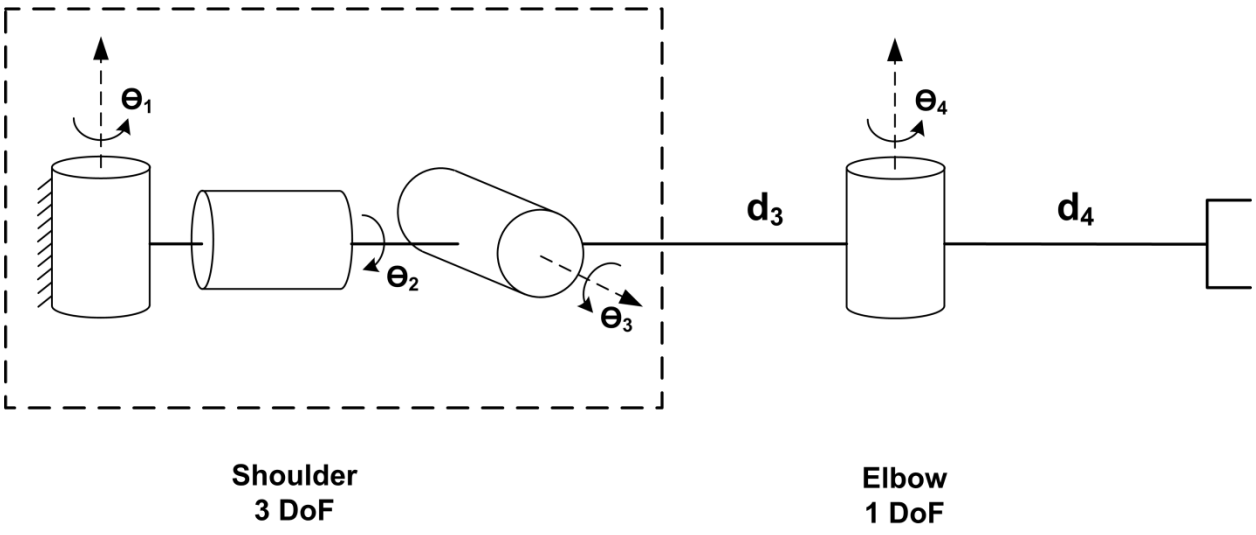

Figure 2-13 – Expanded arm model

The above figure shows how the spherical joint is expanded to three revolute joints, in three perpendicular directions. In order to obtain the same results as the original arm model, the distance between those three joints (shoulder) is set to zero in the equations. The length of the two parts of the arm are d_3 and d_4.

Having the simplified model of the arm, one can write the homogenous transformation matrix that returns each point on the arm in the global frame. It should be noted that the center of the spherical joint is assumed to be the origin of the global frame.

Two transformation matrices have to be obtained in order to find the local position of a point on the arm in the reference frame. Each transformation matrix gives the position of the local point in the specific reference frame. The equation below shows how the transfer matrices work.

$$\mathbf{p}_a^a = \mathbf{H}_b^a \mathbf{p}_b^b \tag{2-20}$$

The transformation matrix $\mathbf{H}_{\mathrm{b}}^{\mathrm{a}}$ converts vector $\mathbf{p}_{\mathrm{b}}^{\mathrm{b}}$ to $\mathbf{p}_{\mathrm{a}}^{\mathrm{a}}$. In general form, $\mathbf{p}_{\mathrm{j}}^{\mathrm{i}}$ is a vector with respect to frame j, expressed in frame i. In other words, the transformation matrix converts a vector which is with respect to frame b and expressed in frame b, to a vector that is with respect to the frame a and expressed in frame a.

The figure below shows the above concept.

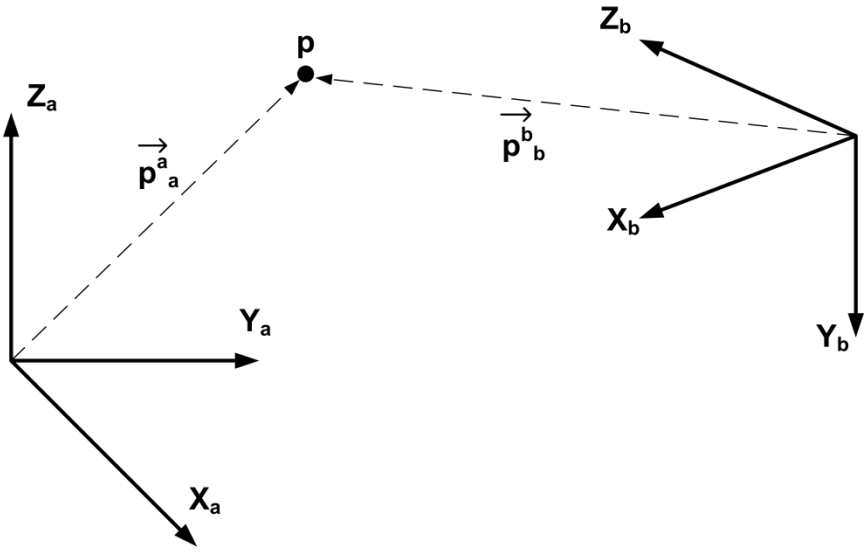

Figure 2-14 – Schematic view of vector definition

Each transformation matrix contains two parts of rotation and translation. The equation below shows a transformation matrix in general form.

$$\mathbf{H} = \begin{bmatrix} \mathbf{R}_{3\times3} & \mathbf{d}_{3\times1} \\ 0 \quad 0 \quad 0 & 1 \end{bmatrix} \tag{2-21}$$

The dimension of a transformation matrix is 4-by-4. $\mathbf{R}_{3\times3}$ is the rotation matrix and $\mathbf{d}_{3\times1}$ is the translation vector.

According to Figure 2-13, the reference frame of the arm's first link is located at the center point of the spherical joint; therefore the first transformation matrix only involves rotation. The equation below shows the transformation matrix of the first part.

$$\mathbf{H}_3^0 = \begin{bmatrix} & & & 0 \\ \mathbf{R}_{z\theta_1}\mathbf{R}_{x\theta_2}\mathbf{R}_{y\theta_3} & & & 0 \\ & & & 0 \\ 0 & 0 & 0 & 1 \end{bmatrix} \tag{2-22}$$

where $\mathbf{R}_{\mathrm{mn}}$ is a transformation matrix in general that only involves a rotation with an angle of n occurred about the m axis.

The transformation matrix of the second part includes translation as well, since the reference frame is located at the elbow. The magnitude of translation is equal to d_3. The equation below shows the second transformation matrix.

$$\mathbf{H}_4^3 = \begin{bmatrix} \mathbf{I_{3\times3}} & \mathbf{d}_{xd_3} \\ 0 \quad 0 \quad 0 & 1 \end{bmatrix} \begin{bmatrix} & & & 0 \\ \mathbf{R}_{z\theta_4} & & & 0 \\ & & & 0 \\ 0 & 0 & 0 & 1 \end{bmatrix} \tag{2-23}$$

where $\mathbf{d}_{xd_3}$ is a transformation matrix which only involves translation with magnitude of d_3 along x direction.

It should be noted that transformation matrix $\mathbf{H}_4^3$ transfers a point in the reference frame 4 to reference frame 3. However, by multiplying the second transformation matrix by the first transformation matrix, the result is a new transformation matrix that returns the point directly in the global frame ($\mathbf{H}_4^0$). The equation below shows how the new transfer function is derived.

$$\mathbf{H}_4^0 = \mathbf{H}_3^0\mathbf{H}_4^3 \tag{2-24}$$

By now, one can determine a point expressed and located on each part of the arm in the global frame according to Figure 2-13.

According to

Table 2-1, the mechanism has to have at least 5 actuators and at least 2 of them have to actuate the second part of the arm. The model which was assumed for this study is to attach 2 cables to the first part and the rest (3) of them attached to the second body. This is also shown in Figure 2-3.

The position of each point on the arm is determined as shown in Table 2-2. It should be noted that the position of each point is expressed in the link reference frame. Also, as was previously mentioned, each body is a cylinder with a radius of 2 cm. Therefore, the position of each point is described in cylindrical coordinates with respect to the local frame.

Table 2-2 – Local position of cable points on the arm in cylindrical coordinate system

	$\mathbf{p_1}$	$\mathbf{p_2}$	$\mathbf{p_3}$	$\mathbf{p_4}$	$\mathbf{p_5}$
Length l (mm)	24	27.5	5	8	26
Angle α (deg)	90	-90	0	90	0

The points $\mathbf{p_1}$ and $\mathbf{p_2}$ are located on the first body and the other points are located on the second body.

The position of each point in its local reference frame is according to equation below.

$$\mathbf{p} = [l \quad r\cos\alpha \quad r\sin\alpha \quad 1]' \tag{2-25}$$

Therefore, if the point is located on the first body, the position in the global frame can be obtained from:

$$\mathbf{p}_0^0 = \mathbf{H}_3^0\mathbf{p}_3^3 \tag{2-26}$$

Similarly, for the second body

$$\mathbf{p}_0^0 = \mathbf{H}_4^0\mathbf{p}_4^4 \tag{2-27}$$

The resultant point is $\mathbf{r}_i$ according to equation (2-9). The $\mathbf{u}_i$ are found from:

$$\mathbf{u}_i = \frac{(\mathbf{p}_{\mathbf{C_i}} - \mathrm{r}_i)}{|(\mathbf{p}_{\mathbf{C_i}} - \mathrm{r}_i|} \tag{2-28}$$

Having all $\mathbf{r}_\mathrm{i}$ and $\mathbf{u}_\mathrm{i}$, one can easily find matrix $\mathbf{A}$. It should be noted that the joint variables which were noted as $\mathrm{q_i}$ previously are shown as θ_i in Figure 2-13. MATLAB code was developed to derive the components of matrix $\mathbf{A}$. All the vectors are ewith respect to and expressed in the global coordinate system.

Now, a workspace has to be defined for the robot that is suitable for rehabilitation. The workspace that was considered for this study is shown in the table below. It should be noted that the workspace is given in joint variables and since they are angles of rotations, their units are in degrees.

Table 2-3 – Workspace of the rehabilitation mechanism

	q_1	q_2	q_3	q_4
Minimum Value (deg)	-20	-20	0	0
Maximum Value (deg)	20	0	20	90

The above table describes the workspace in the joint variables, so according to the "workspace tensionability" section, one can evaluate the tensionability of the given workspace using the algorithm shown in Figure 2-10.

The last step is to define a space for the positioning of each actuator and eventually Design Parameter Space. Figure 2-15 shows the possible positions of each actuator based on Figure 2-4. The dark areas are the regions considered for each actuator.

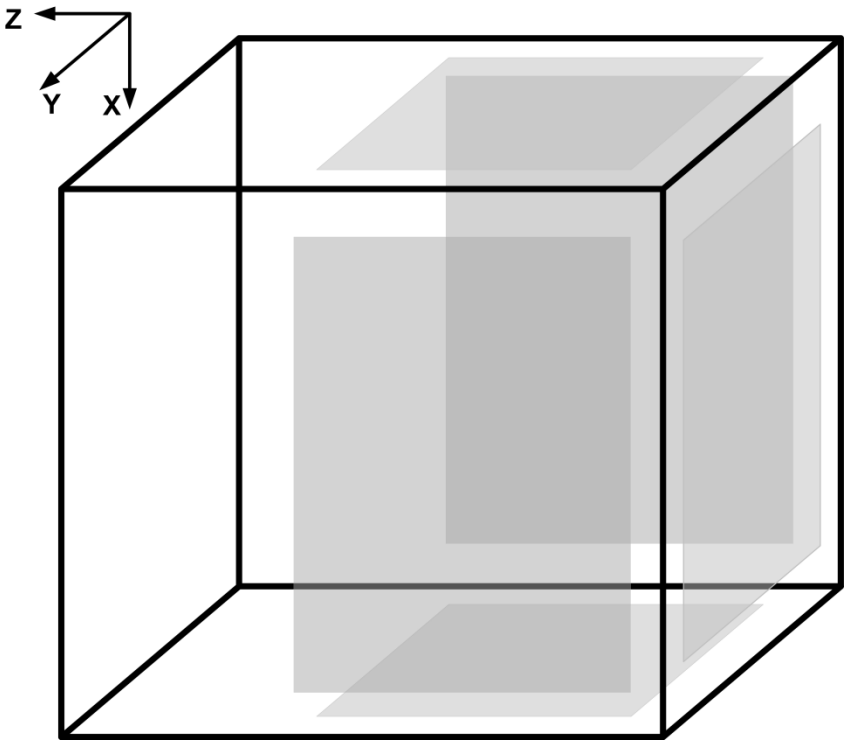

Figure 2-15 – Considered region as the Design Parameters Space

According to Figure 2-15, the shaded areas were chosen as the Design Parameters space. The reason for only choosing a part of each plane is the location of the beam that holds the arm. If the actuators were placed somewhere other than the shaded area on the planes, there would likely be interference between the cables and the beam.

Also, the actuator can only move within the planes. This means each actuator only has two adjustable parameters. For instance, the actuator that is placed on the front plane, has its y-coordinate fixed, so only x, z-coordinates are design parameters.

The table below determines the numbering of actuators and their design parameters based on their planes.

Table 2-4 – Actuators and their design parameters

Actuator	Plane	Fixed component	Design Parameters
2	Front	y	x_2, z_2
3	Top	x	y_3, z_3
4	Right	z	x_4, y_4
6	Bottom	x	y_6, z_6
7	Back	y	x_7, z_7

According to the table above, there are 10 design parameters. Therefore, the dimension of the Design Parameter Space is 10. The table below shows the range of each dimension of the Design Parameter Space. All the dimensions are in millimeters.

Table 2-5 – Design Parameters Space

	x_2	z_2	y_3	z_3	x_4	y_4	y_6	z_6	x_7	z_7
Min. (mm)	-400	-600	-600	-600	-400	-600	-600	-600	-400	-600
Max. (mm)	400	100	600	0	1000	600	600	0	400	100

Also, the value of the fixed component for each actuator is listed in the table below.

Table 2-6 – constant component of each actuator

	Actuator 2	Actuator 3	Actuator 4	Actuator 6	Actuator 7
Fixed Component Value (mm)	y_2 =-897	x_3 =-592	z_4 =-792	$x_6 = 897$	$y_7 = 1207$

Having the desired workspace and Design Parameter Space, one only needs to determine the step-sizes for both, to be able to implement the synthesis algorithm.

The step-sizes considered for workspace and Design Parameter Space were $h_i = \left(\frac{q_{i_{max}} - q_{i_{min}}}{4}\right)$ and $g = 20\ (cm)$ respectively.

2.6 Results of the Synthesis Optimization

MATLAB code was developed based on the algorithm introduced in Figure 2-11. There are three separate functions for each part. The first evaluates tensionability of a single point in the work space. The second checks the tensionability of a given workspace by testing all grid points of the workspace using the first function. The last finds those set of parameters that make the mechanism tensionable for the desired workspace. The third function uses the second one for each grid point of the Design Parameter space.

The code was run for the input data presented in Table 2-3 and Table 2-4. All feasible configurations for the robot were found. However, the best one is yet to be chosen which has the best performance.

As previously stated, the best solution is the one that has the minimum variance in the components of $\mathbf{n}$. $\mathbf{n}$ is the null vector of matrix $\mathbf{A}$. It was discussed in the previous section as to why the cost function was chosen as the variance of $\mathbf{n}$.

The solution that has the minimum value of the cost function was set as the initial point of the gradient-based minimization process. That set of the design parameters that correspond to the minimum cost function is shown in the table below.

Table 2-7 – The grid point that has the minimum value of cost function amongst all the grid points

Param.	x_2	z_2	y_3	z_3	x_4	y_4	y_6	z_6	x_7	z_7
Value (cm)	0	15	-40	0	60	40	-40	0	-40	0

According to Figure 2-12, the grid point that should be set as the initial point of optimization has already been found and mentioned in Table 2-7. This point was considered for the initial point of the gradient-based optimization. The gradient vector guides the optimization towards the point which has probably the minimum value within the Design Parameter Space. A MATLAB code was developed that takes the initial point of the optimization and the boundary of space as well. It returns the point that has the minimum value for a specific function. The resultant point is shown in table below.

Table 2-8 – The point that has minimum cost function value inside the Design Parameter Space

Param.	x_2	z_2	y_3	z_3	x_4	y_4	y_6	z_6	x_7	z_7
Value (cm)	25.65	14.94	-31.51	-0.06	-11.00	59.96	-39.95	10.00	-42.88	0

According to Table 2-8 and Table 2-6, the final positions of the actuators are determined as:

Actuator Number	**Position (cm)**
2	[25.65,-89.70,14.94]
3	[-59.20 -31.51 -0.06]
4	[-11.00 59.96 -79.20]
6	[89.70 -39.95 10.00]
7	[120.70 -42.88 0]

Having the position of all the actuators they were installed on the frame. However, the real positions of the actuators after the installation are not exactly the same as the theoretical values. Therefore, the actual positions of the actuators need to be identified using a method that is explained in the next chapter.

3 Kinematic Modeling and Parameter Identification

Since the fabricated mechanical parts and their assemblies do not have necessarily exactly the same dimensions as what are specified in drawings, every robotic system needs to undergo parameter identification or calibration. Although all the parameters of the system are already determined according to the design procedure detailed in chapter 2, in the real world, the outputs of the system depend on the real values of the parameters of the system, such as positions and lengths of the mechanical parts.

3.1 Introduction

As mentioned before, the main goal of this study is to present a reconfigurable rehabilitation mechanism. Since different rehabilitation tasks are to be performed on patients, the mechanism has to be reconfigured by relocating its cable actuators such that the new desired workspace is provided. After this relocation is done, the accurate positions of the cable actuators need to be identified (i.e., the kinematic model is calibrated).

It is assumed that the radii of pulleys are known. Also, the sensors do not have any nonlinearity. The potential problem of the proposed method in the real world system can be due to the mentioned assumptions that were taken in the theory.

3.2 Method Description

A method of parameter identification or kinematic model calibration is chosen for this study that uses the robot sensors. This helps the operator to identify parameters of the mechanism without needing technical knowledge or any other equipment. Also, it decreases the initial setup time.

As shown in Figure 2-1, the calibration problem here can be understood as finding the accurate location of each cable actuator. This is done by using the known position of several auxiliary points such as P1 to P4

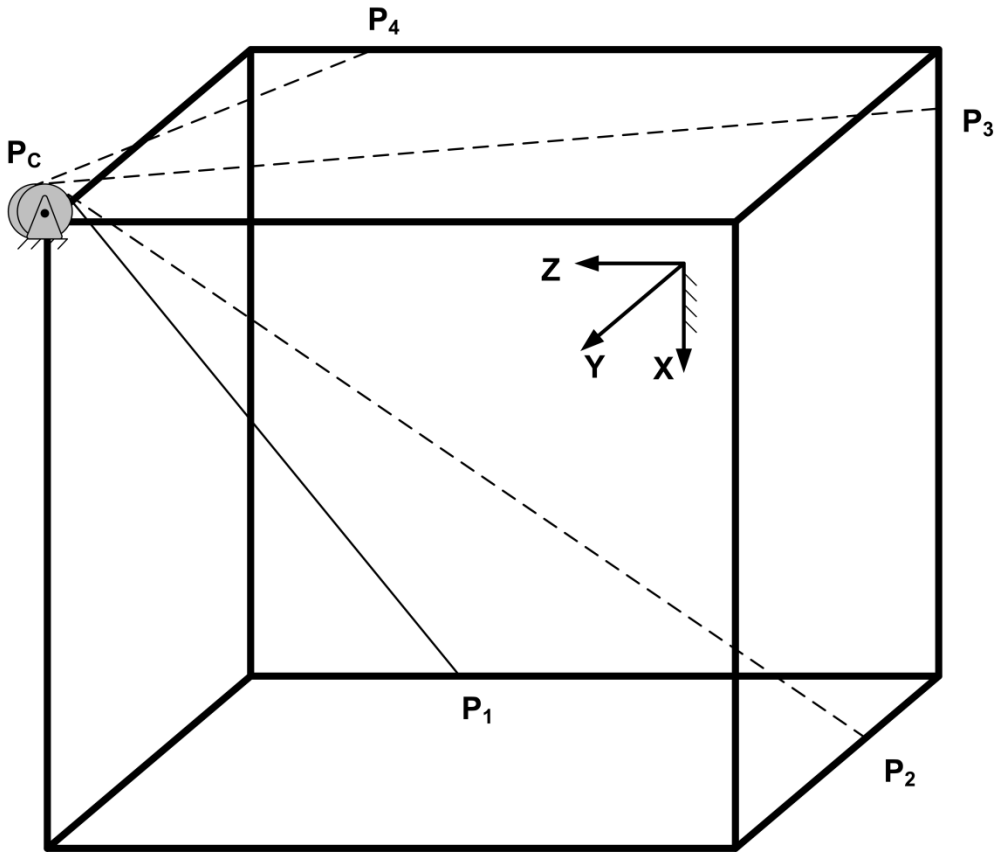

Figure 3-1 – Schematic view of identification problem

The coordinate of the actuator is shown as $\mathbf{P}_C$, which is unknown and needs to be identified. Also, some known points are perfectly located on the frame and act as auxiliary points. They are constant for all the cases and independent of location of actuators. These points are shown as $\mathbf{P}_i$. It will be shown in the next sections that why 4 known points are needed to have a unique solution to this problem.

The procedure is described briefly as following according to Figure 3-1:

1. The operator puts the free end of the cable on $\mathbf{P}_1$ and reads the number that the encoder shows.
2. Then the operator takes the free end of the cable to another point other than $\mathbf{P}_1$ (e.g. $\mathbf{P}_2$). The cable should be tensioned during the process to ensure that the cable is not slipping on the encoder's shaft. In other words, the actuator has to pull the cable.
3. The user reads the number that the encoder is showing.
4. The difference between the two recorded numbers represents the difference between the distances of each known point and the actuator as unknown points.
5. The operator repeats steps 1-4 for all the points.

6. Based on the obtained data and the geometry of the system, the position of the unknown point (actuator positions) can be found. The mathematical equations for solving the identification problem are presented in the upcoming sections.

The above procedure requires no external sensor or equipment for parameter identification. The measuring task is supposed to be done by the system sensors.

After collecting all the required data as above, the operator has to put the data into a set of equations and solve them. Later in this chapter, it will be explained that the equations are non-linear and a numerical method is used to solve them.

The distance between fixed points should not be too short compared to the size of the system. A Short distance may cause inaccurate results since the equations will be solved using numerical methods. Considering a simple problem below explains the reasoning of this statement.

Assume that finding the position of an unknown point in a plane is desired and two auxiliary points are given. We want to use the same procedure of this study to solve the problem. As it is shown in Figure 3-2, the known points are assumed to be too close to each other in comparison with their distances to the unknown point. In this case, the geometry becomes similar to two radii of a circle. Therefore, we have little change in the cable length moving from one point to another and as a result, there will no way to distinguish between the two points.

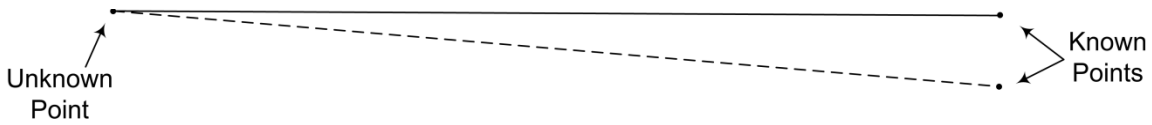

Figure 3-2 – Two known and one unknown points

Also, measurement error exists in all physical systems and this error will have its effects on the final results. Therefore, verification should be done using a reliable source in order to make sure that the method gives appropriate answers.

3.3 Kinematic Modeling

To derive the required equations, first the model of actuators and geometry of the system should be presented. The figure below shows the drawing of the actuator case and the motor that been installed on the case.

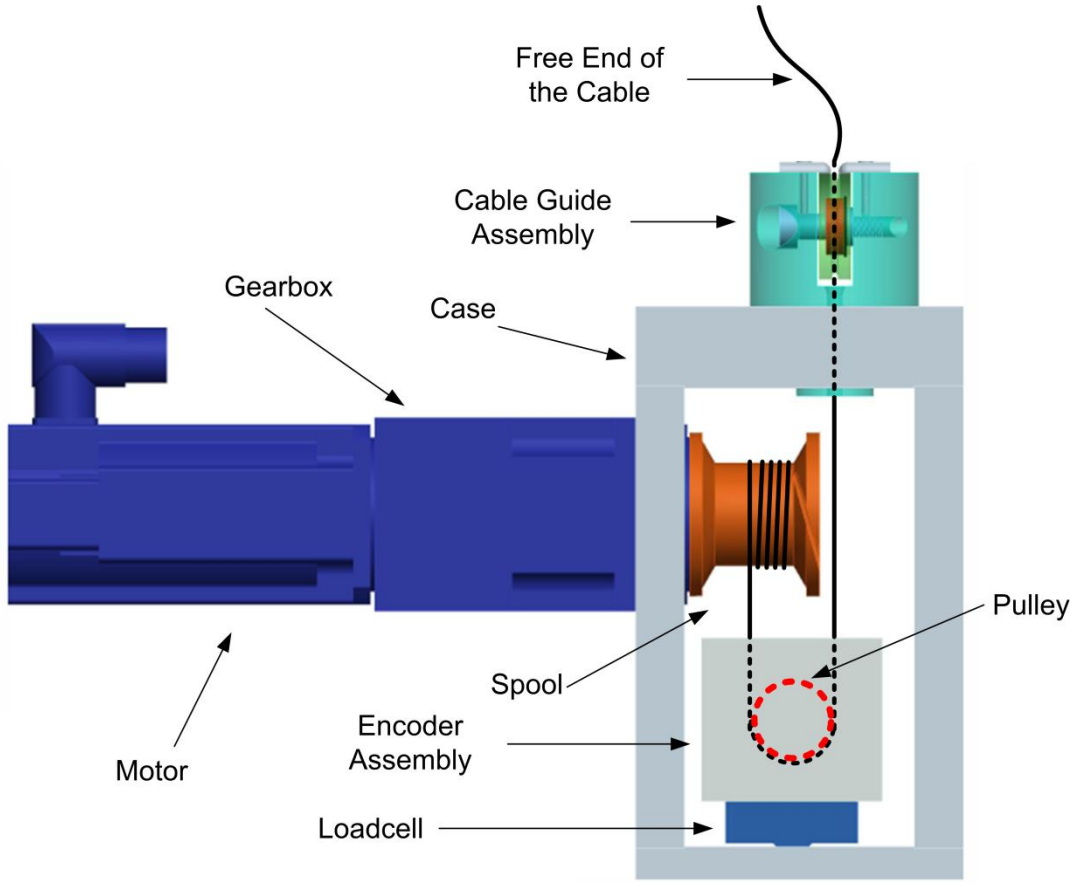

Figure 3-3 – Drawing of the actuator case

Figure 3-4 shows the fabricated and assembled actuator's case.

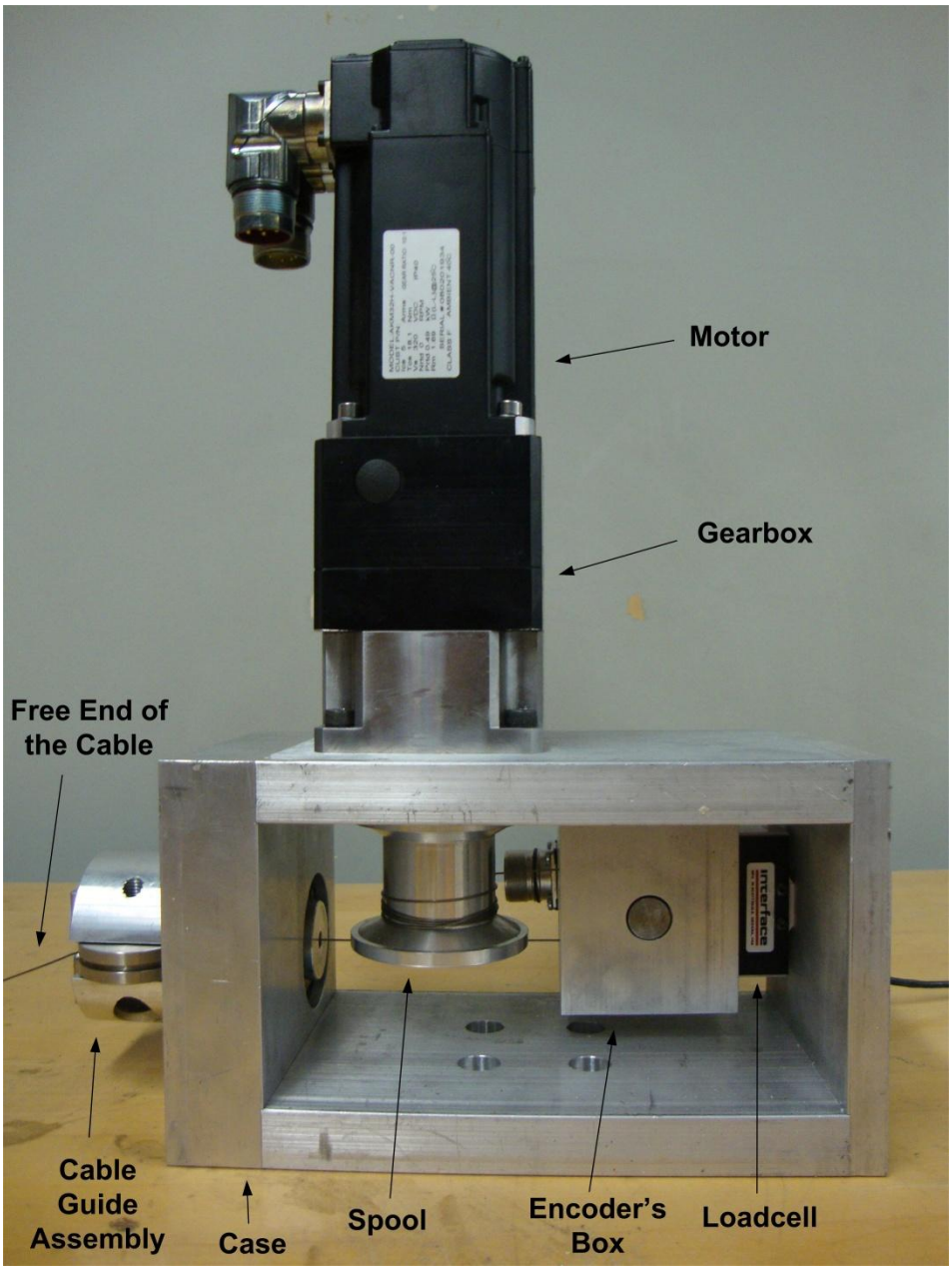

Figure 3-4 – photograph of the fabricated actuator case

One needs to take a point along the cable as the fixed end of it. This assumption is required to develop the equations, as will be discussed in the next sections. To claim a point as the fixed end of the cable, the side view of the cable guide assembly is shown in Figure 3-5.

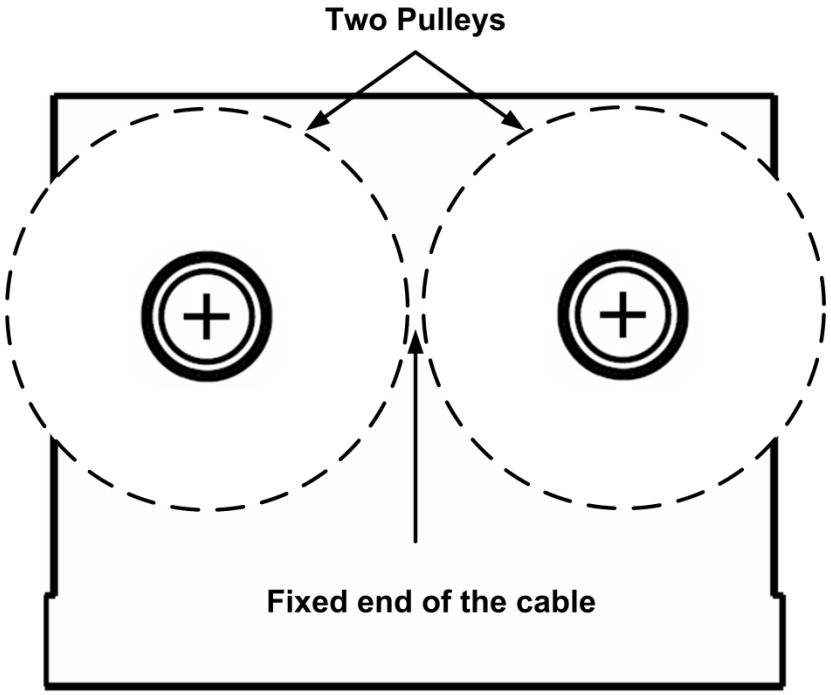

Figure 3-5 – Schematic side view of the cable guide assembly

The cable guide assembly is shown in Figure 3-5.

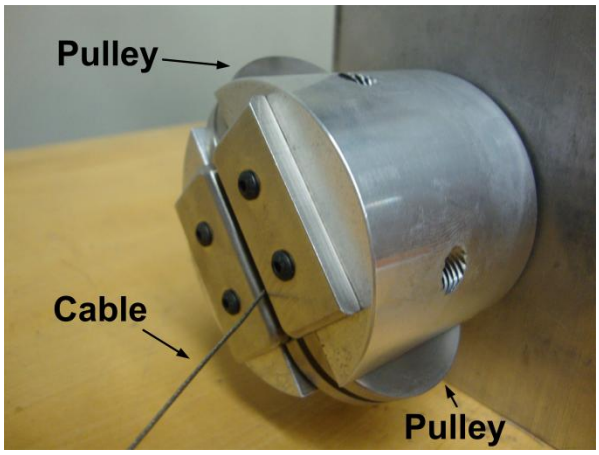

Figure 3-6 – Close view of cable guide assembly

3.4 Governing Equations

According to Figure 3-5, the point that is taken as the fixed end of the cable is exactly in the middle of pulley centers. Since the point is surrounded by the two pulleys and there is no space for the cable to deviate from that point, one can claim it as the fixed end of the cable with an acceptable accuracy.

A parameter identification procedure requires a number of known points. In this case, these points are located on different points around the frame of the robot and are called known points (P_i). One end of the cable is placed on the first known point (P_1), and then moved to the i^{th} known point. The user saves both corresponding values of the encoder at P_1 and P_i. The difference between these values is noted as d_i. In other words, if we assume that l_i represents the length of the cable between the fixed end of it and P_i, then d_i represents the difference between l_1 and l_i.

During this process the cable must remain taut. To find the position of each actuator (the point that was assumed as the fixed end of the cable previously), three equations are solved since the type of system is spatial (the unknown point has three components). To have three independent equations in terms of d_i, four known points should be taken ($i = 1,2,3,4$). Because at least four cables are needed due to the nature of the mechanism and how the data are collected.

The figure below shows the parameters and unknown values. It should be noted that this figure only includes one of the two pulleys in the cable guide assembly.

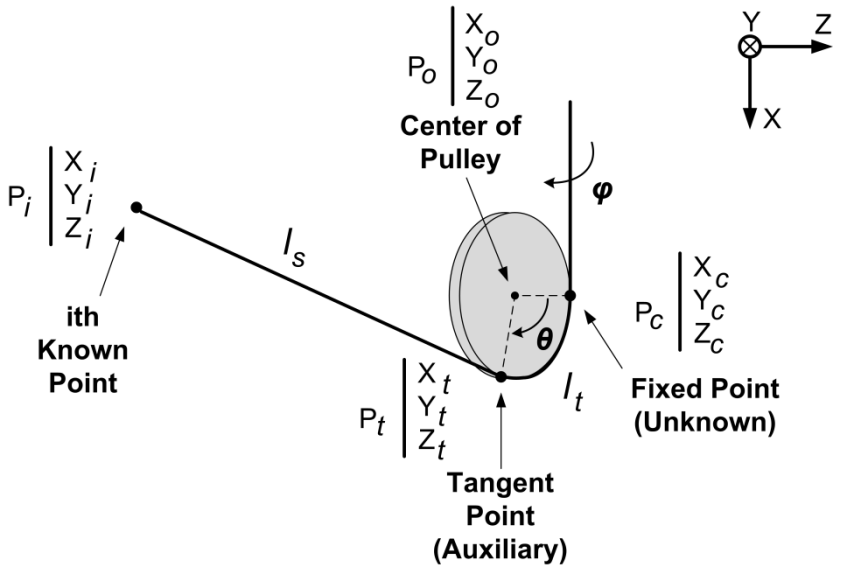

Figure 3-7 – Schematic view of parameter identification problem

According to the figure above and provided explanations, the following equation could be written:

$$l_1 - l_i = d_i; \tag{3-1}$$

where l_i is the length of cable between fixed point and i^{th} known point.

The above equation is not sufficient to determine P_C (the fixed end of the cable) since the cable between P_C and P_i consists of two parts. One is the part that bends around the pulley and the other part is straight from the tangent point towards P_i (by neglecting the cable sagging). Therefore, according to Figure 3-7, Eq. (3-1) breaks down into the following expanded equations:

$$l_{s_1} + l_{t_1} - \left(l_{s_i} + l_{t_i}\right) = d_i; \quad i = 2,3,4 \tag{3-2}$$

where l_{s_i} and l_{t_i} are straight and curved parts of cable respectively.

One can write l_s and l_t in terms of the components of P_t:

$$l_s = \sqrt{(x_t - x_i)^2 + (y_t - y_i)^2 + (z_t - z_i)^2} \tag{3-3}$$

$$l_t = R\theta \tag{3-4}$$

where x_t, y_t, and z_t are components of P_t. Also, R is the radius of the pulley and θ is the corresponding angle of the curved part of the cable. All the mentioned parameters are shown in Figure 3-7.

One can easily find θ in terms of P_t and P_C and rewrite Eq. (7) as follow:

$$\sin\theta = \frac{|\overrightarrow{(\mathbf{P}_t - \mathbf{P}_o)} \times \overrightarrow{(\mathbf{P}_c - \mathbf{P}_o)}|}{|\overrightarrow{(\mathbf{P}_t - \mathbf{P}_o)}| \times |\overrightarrow{(\mathbf{P}_c - \mathbf{P}_o)}|}; \ \cos\theta = \frac{\overrightarrow{(\mathbf{P}_t - \mathbf{P}_o)}.\overrightarrow{(\mathbf{P}_c - \mathbf{P}_o)}}{|\overrightarrow{(\mathbf{P}_t - \mathbf{P}_o)}| \times |\overrightarrow{(\mathbf{P}_c - \mathbf{P}_o)}|}$$
$$l_t = R \times atan2(\sin\theta, \cos\theta) \tag{3-5}$$

By now, an expanded version of Eq. (3-1) has been developed, but three unknown parameters still exist in this new equation. In order to solve the problem, one needs to develop three more equations and solve them simultaneously with the main equations. Although the goal is to find the values of x_c, y_c, and z_c, obtaining by position of the tangent point is necessary, since it has been introduced to the set of equations.

Another parameter should be introduced since it will be used frequently later on in this study. As the pulley can rotate about X-axis of the coordinate system, a revolution angle should be considered to describe the angular position of the pulley in that direction. This angle is shown as φ in both Figure 3-7 and Figure 3-8, which is the top view of the pulley.

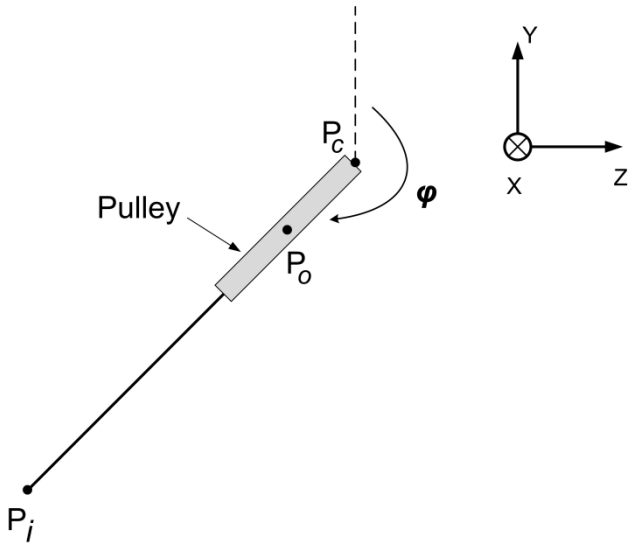

Figure 3-8 – Schematic top view of the parameter identification problem

This angle is measured with respect to the positive direction of Y-axis about X-axis. The shown coordinate system is global. One can write an equation for φ in terms of P_i and P_c as shown below:

$$\cos\varphi = \frac{y_i - y_c}{\sqrt{(x_i - x_c)^2 + (y_i - y_c)^2 + (z_i - z_c)^2}}$$

$$\sin\varphi = \frac{z_i - z_c}{\sqrt{(x_i - x_c)^2 + (y_i - y_c)^2 + (z_i - z_c)^2}} \tag{3-6}$$

$$\varphi = atan2(\sin\varphi, \cos\varphi)$$

Angle φ is defined based on the assumption of the coordinate system and the pulley rotates about one of the main axes for all the actuators.

According to Figure 3-8, one can easily find the position of the pulley's center.

$$P_o = P_c + R\begin{bmatrix} 0 \\ \cos\varphi \\ \sin\varphi \end{bmatrix} \tag{3-7}$$

According to the above explanations, it is clear that now the problem has 15 unknowns and the other parameters can be written in terms of these 15 unknowns. The unknowns are the components of P_c and P_{t_i} ($i = 1,2,3,4$). Therefore, 15 equations are needed to obtain a unique set of answers for this algebraic problem. Based on equations (3-2), (3-3), and (3-4), three of them are already developed.

According to presented material in the previous section, there are four (we have four known points) groups of three equations for tangent points and each group is to be written independently.

Below is the procedure to show how each equation in a group is derived. It should be noted that three equations below will be derived for $i = 1,2,3,4$ and this means 12 equations will be derived.

1) The first equation is to state that P_t is on the pulley perimeter:

$$|P_t - P_o| = R \tag{3-8}$$

which means that the distance between the tangent point (P_t) and the center of the pulley (P_o) is equal to the radius of the pulley. R is Accurately known.

2) The second equation is obtained from the fact that the line connecting P_t and P_o is perpendicular to the cable.

$$\overrightarrow{(P_t - P_o)}.\overrightarrow{(P_t - P_i)} = 0 \tag{3-9}$$

3) The last equation ensures that P_t lies on the pulley plane or:

$$(z_t - z_t)\cos\varphi - (y_t - y_t)\sin\varphi = 0 \tag{3-10}$$

Now, considering equations. (3-1), (3-8), (3-9), and (3-10) together we have 15 equations, but there are still some terms containing P_o. By substituting P_o from Eq. (3-7) one can rewrite all the mentioned equations only in terms of P_c and P_{t_i} $(i = 1,2,3,4)$.

It should be noted that all the above derivations are based on one particular position and orientation of an actuator, but the same procedure can be applied to the rest by changing the direction of coordinate system's axes. In all the cases, the concept remains the same.

3.5 Implementation of the Identification Method and Results

The last step is to solve equations (3-1), (3-8), (3-9), and (3-10) using a numerical method since they are nonlinear. The equations were solved using Newton-Raphson method. To do so, a MATLAB code including function $fsolve$ was used to solve them numerically. The initial guess of MATLAB code was the values obtained in the synthesis section.

According to the kinematics design section, 5 actuators were considered for this cable-driven mechanism whose locations were identified one by one using this approach.

Based on Figure 3-1 and materials discussed in previous sections, 4 points were taken as the known points. Coordinates of the known points were measured using a Faro arm [34] with

accuracy of up to 18 microns [35]. More details about the Faro arm are discussed in the next section. The table below shows the positions of the known points. The coordinates shown in Table 3-1 are expressed with respect to global frame.

Table 3-1 – Positions of known points

Point	Coordinates (mm)
$\mathbf{P}_1$	[-709.81 1009.18 -909.33]
$\mathbf{P}_2$	[-709.35 -181.20 -985.14]
$\mathbf{P}_3$	[1326.60 -1023.43 -909.33]
$\mathbf{P}_4$	[-708.8726 -1024.8315 -909.3288]

The known points were located on the frame so there was no need to fabricate an extra fixture.

According to the procedure introduced at the beginning of this chapter, the following steps were followed:

1. The free end of the cable was placed on $\mathbf{P}_1$ and then moved to $\mathbf{P}_2$. The difference of initial and final numbers read by the encoders were recorded.
2. The same procedure was done for $\mathbf{P}_1$ and $\mathbf{P}_3$ as well as $\mathbf{P}_1$ and $\mathbf{P}_4$.
3. The cable was tensioned during all steps.

The recorded data is shown in Table 3-2.

Table 3-2 – The d_i's that were read using encoders.

Actuator	d_1 (mm)	d_2 (mm)	d_3 (mm)
2	489.90	-1763.94	-1121.82
3	616.23	-608.25	465.65
4	-262.72	-1423.00	-991.62
6	373.42	1506.82	353.03
7	701.57	1040.66	927.61

4. The recorded value was input to the MATLAB function.

The results are shown in Table 3-3 show the parameter estimation results.

Table 3-3 – Final answers of identification problem obtained from MATLAB code

Actuator	The Resultants Obtained from MATLAB code		
	x_c (mm)	y_c (mm)	z_c (mm)
2	-481.36	894.52	110.44
3	-595.74	-325.30	-000.92
4	-105.60	596.50	-799.39
6	1276.37	-439.06	64.48
7	389.67	919.21	126.95

3.6 Verification of the Method Using a Faro Arm [34]

In order to verify the accuracy of the introduced method, the values shown in Table 3-1 were compared with values measured using a Faro arm.

The Faro arm is a Coordinate Measurement Machine (CMM) that measures the coordinates of a point in the space with respect to another point as the origin. The figure below shows a Faro arm.

Figure 3-9 – A Faro arm

A Faro arm consists of 3 links, which allows the operator to reach a large volume of workspace. Using a probe located at the free end of the arm, the operator touches every point that needs to be measured. The position is calculated based on the length of the links and angle of joints through a forward kinematics analysis of the arm. For instance, in order to measure a plane, the

user only needs to measure 3 points; then the integrated software of Faro arm determines the plane passing through those 3 points. The manufacturer of Faro arm claims accuracy of up to 18 microns [35].

Before measuring the position of the actuators, the origin of the coordinate system was located. It was said previously that the origin of the global coordinate system is at the center of the spherical joint. Therefore, the sphere was determined by measuring 4 arbitrary points located on the spherical joint. The figure below shows 4 arbitrary points on the sphere.

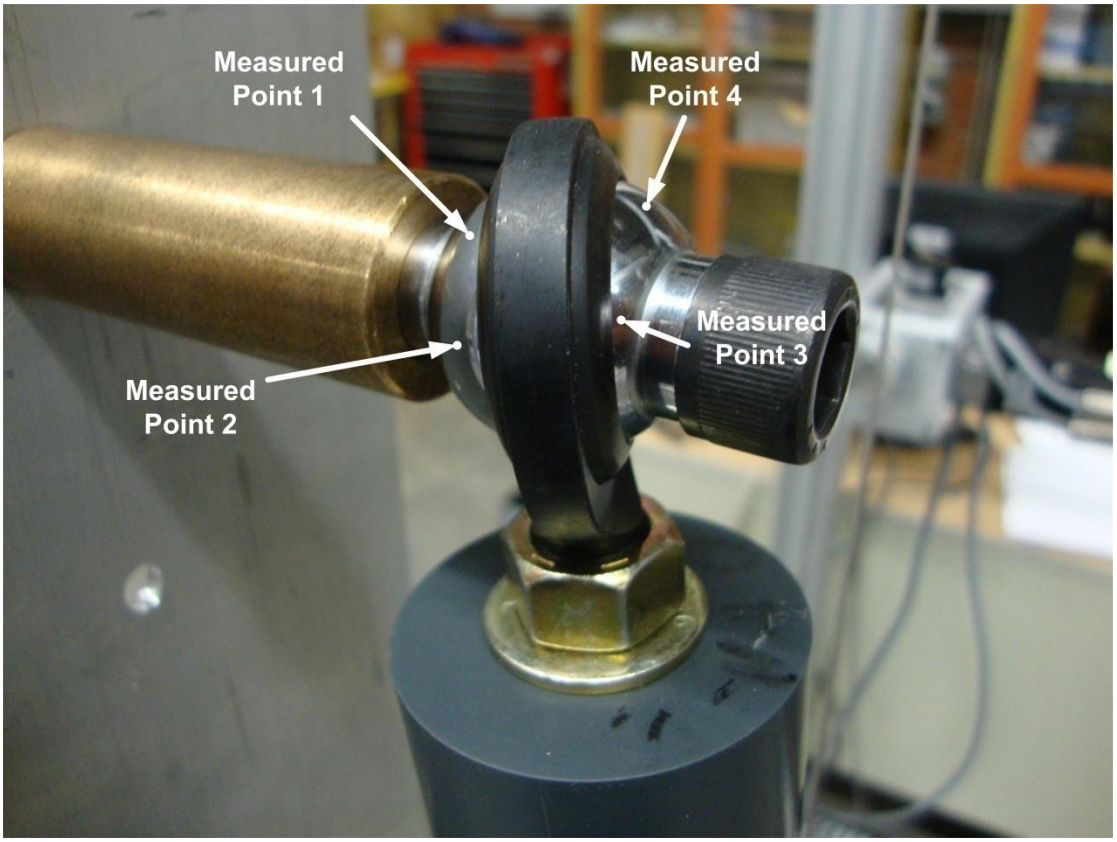

Figure 3-10 – 4 arbitrary points on the spherical joint to determine the origin

As shown in the figure above, the point should not be on the same circle; otherwise, there will be infinite number of answers.

After finding the center point of the spherical joint and defining it as the origin of the coordinate system, the positions of the fixed end of cables (actuators) were measured. According to Figure 3-5, the fixed end of the cable is assumed to be at the middle of the two pulleys in the cable assembly guide. Therefore, it was necessary to find the center of the top surface of the assembly and then find the mentioned point using the provided drawings. First, the surface plane of the cable guide assembly was measured at 3 arbitrary points and it was intersected by the cylinder of the cable guide assembly. The cylinder was measured using

arbitrary points. Figure 3-11 shows how the surface plane and cylinder were measured using the Faro arm.

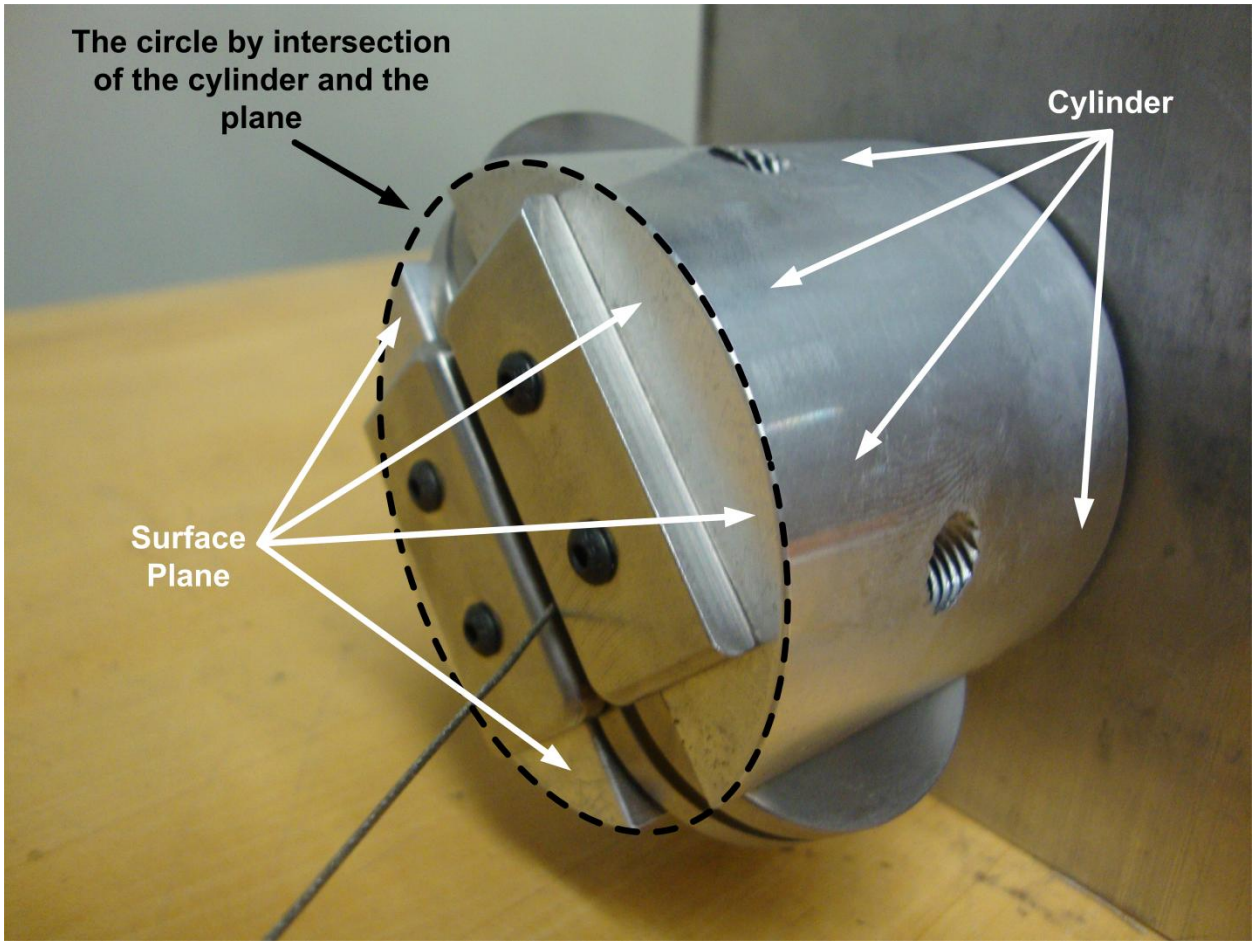

Figure 3-11 –The circle was constructed by intersection of cylinder and surface plane

The dotted shape above shows the circle of the cable guide assembly. In order to find the coordinate of the point in the middle of two pulleys, the drawing below was used.

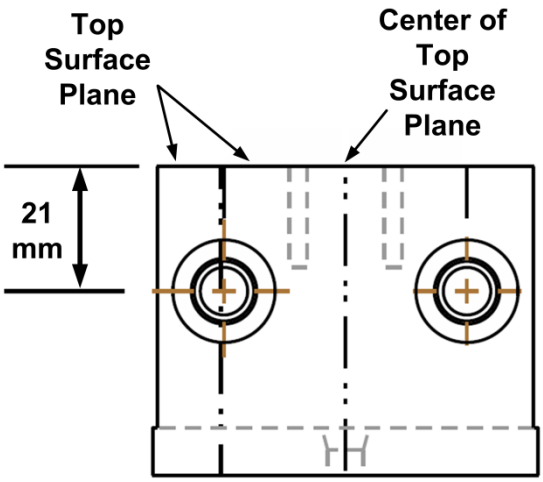

Figure 3-12 – Drawing of cable guide assembly

As shown in the above figure, the assumed fixed end of the cable is located 21 millimeters beneath the top plane. Using the procedure above, all positions of the actuators were measured and shown in Table 3-4, in comparison with the values obtained from the previous section. It should be noted that all the values are given in millimeters.

Table 3-4 – Obtained results using developed code and Faro arm

Actuator	Obtained from Parameter Identification			Faro Arm		
	x_c (mm)	y_c (mm)	z_c (mm)	x_c (mm)	y_c (mm)	z_c (mm)
2	-481.36	894.52	110.44	-481.92	895.64	111.54
3	-595.74	-325.30	-000.92	-595.56	-325.04	-1.166
4	-105.60	596.50	-799.39	-105.96	596.49	-799.66
6	1276.37	-439.06	64.48	1277.22	-438.00	63.72
7	389.67	-919.21	126.95	389.85	-918.50	127.64

Table 3-5 shows the absolute error value of each coordinate.

Table 3-5 – Absolute error values of actuator coordinates

Actuator	Absolute error of x_c (mm)	Absolute error of y_c (mm)	Absolute error of z_c (mm)
2	0.56	1.12	1.1
3	0.18	0.26	0.246
4	0.36	0.01	0.27
6	0.85	1.06	0.76
7	0.18	0.71	0.69

According to the values above, the maximum error is 1.12mm and the minimum error is 0.01mm. Also, the average of all the error values is 0.26mm which indicates an acceptable accuracy. Note that the error between the actual position and obtained value (measured using Faro arm) can be neglected compared to the size of the mechanism. Since the size of the mechanism is in order of 2m then an error of 1mm is an acceptable number. In other words, the errors are called acceptable compared with the size of the mechanism.

4 Control

This chapter introduces a method of control for cable-driven mechanisms. The control will be then developed for the cable-driven mechanism being considered in this thesis when working with the upper arm of human body for rehabilitation purposes.

The studied mechanism in this chapter is a cable robot that does the rehabilitation task of a shoulder model. The mechanism has 3 degrees of freedom and needs to be actuated by 4 motors. A MATLAB Simulink model is made and the results of controller implementation will be presented at the end.

After designing the configuration of the mechanism for the required workspace and identifying the actual values of the kinematic parameters, a controller has to be implemented. Remember that this mechanism has been designed to follow a desired trajectory, provided by the therapist. The therapist indicates the trajectory by moving the arm through an appropriate path and the mechanism is supposed to save the data using its sensors. Then the robot has to repeat the same trajectory in order to complete the rehabilitation process. Collecting data and learning the trajectory is being done in a different thesis. The present work assumed the trajectory is provided and therefore develops the control for repeating the trajectory.

Since the present application requires a delicate interaction between the robot and human, we needed to select a control strategy that enables us to determine and provide a desired level of comfort for the patient while performing a trajectory tracking task. For this reason, impedance control was chosen which is briefly explained in the next section. Also, position control can be used which is not addressed in this thesis.

4.1 Impedance Control

The main concept of impedance control is to find the value of actuation forces such that the end-effector acts as a mass-spring-damper system. In this type of control method, impedance of the system is set by assigning the coefficients of virtual inertia, damping and stiffness elements. The desired performance of the controlled mechanism should represent the impendence of a mass-spring-damper system.

A simple system with one degree of freedom is shown below.

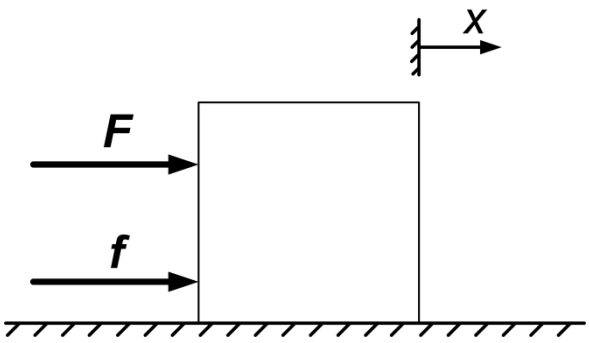

Figure 4-1 – A simple one degree of freedom system

The goal is to find value of F so the body follows the desired trajectory $\mathrm{x_d}$ and performs as a mass-spring-damper system. In other words, the actuator is applying the force F so that the system can follow the desired trajectory and act as a mass-spring-system to the environment. Neglecting any friction force, the dynamic equation for the system shown in Figure 4-1 is:

$$F = m\ddot{x} - f \tag{4-1}$$

where m is the body mass and f is the external force that the environment is applying on the system. In other words, the user who is interacting with the system applies the force f. Also, F is the force applied by the actuator.

According to impedance control theory [36], the user should feel such that he/she is interacting with a mass-spring-damper. Therefore the interaction force f is determined using the following equation by the controller:

$$f = M_e(\ddot{x_d} - \ddot{x}) + B_e(\dot{x}_d - \dot{x}) + K_e(x_d - x) \tag{4-2}$$

where M_e, B_e, and K_e are the desired impedance coefficients set by the user.

In fact, if the controlled system deviates from the desired trajectory due to some external disturbances, the control action (the force value) changes such that the system acts as a mass-spring-damper to the environment. In other words, the user who interacts with the mentioned system feels the reaction force of a mass-spring-damper system with acceleration of$(\ddot{x_d} - \ddot{x})$, velocity of $(\dot{x}_d - \dot{x})$, and displacement of $(x_d - x)$. The mass inertia of such a system is M_e, the damping coefficient of it is B_e, the user feels a stiffness is equal to K_e. It is obvious that when the system is following the exact desired trajectory, the value of f is zero. This means that when the system is not following the trajectory, the controller forces it to the desired values of acceleration, velocity, and position; and by getting closer to the desired values, the magnitude of force f decreases.

In a control cycle, when the user applies force $\bar{f}$ to the system, he/she causes it to deviate from the desired trajectory. The sensors read the actual position, velocity, and acceleration of the system, and pass the data on to the controller. The controller then calculates the interacting force f that a mass-spring-damper system would apply to the environment based on the captured data by the sensors. Having the interacting force and the dynamic equation of the system, the controller determines the force that the actuator has to apply to the system such that the interacting force between the system and the environment becomes f.

In summary, the controller takes the values of position, velocity, and acceleration from the sensors and calculates the interacting force using equation (4-2) and puts it into equation (4-1) to find the value of actuator force F. Then the actuator applies a force with a value of F on the system as the actuation force.

According to the above, the interacting force that is determined by the controller f and the actual force $\bar{f}$ are not essentially equal.

One can extend the concept above to a n_{DoF} degrees of freedom system. In this case, following the Lagrange notation, the scalar force is replaced by the vector of n generalized forces. Each force is related to corresponding generalized coordinate. For instance, Figure 4-2 shows a three degrees of freedom system.

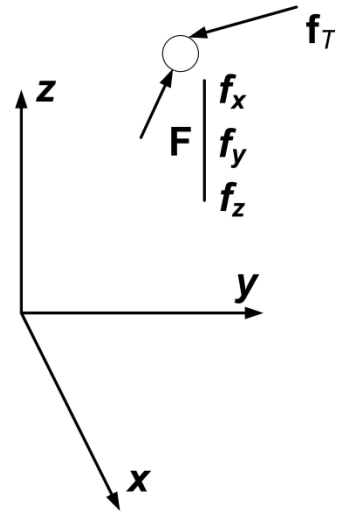

Figure 4-2 – A three degrees of freedom system with single body

As shown in the figure above, the applied force is a vector of three generalized forces. Each component corresponds to a generalized coordinate.

The dynamic equation for the system shown in Figure 4-2 is:

$$\mathbf{F} = m\ddot{\mathbf{p}} - \mathbf{f}_T \tag{4-3}$$

where p is the position of the body in the Cartesian coordinate system, and m is the body's mass, and f is the interaction force between the system and the environment.

Again, according to the concept of impedance control, the values of generalized forces are obtained from:

$$\mathbf{f}_T = \mathbf{M}(\ddot{\mathbf{p}}_d - \ddot{\mathbf{p}}) + \mathbf{B}(\dot{\mathbf{p}}_d - \dot{\mathbf{p}}) + \mathbf{K}(\mathbf{p}_d - \mathbf{p}) \tag{4-4}$$

where $\mathbf{p}_d$ represents the desired trajectory.

In this case, $\mathbf{f}$ is a vector of three generalized forces

$$\mathbf{f} = [f_x \quad f_y \quad f_z]' \tag{4-5}$$

and so, the impedance coefficients are 3-by-3 matrices:

$$\begin{gathered} \mathbf{M} = [m_{ij}] \\ \mathbf{B} = [b_{ij}] \\ \mathbf{K} = [k_{ij}] \\ i, j = \{x, y, z\} \end{gathered} \tag{4-6}$$

In the equations above, m_{ij} is the inertia that corresponds to the generalized coordinate i, when the acceleration of generalized coordinate j deviates from its desired value. The same definition is applicable for damping coefficients b_{ij} and stiffness coefficients k_{ij}.

According to equations (4-4) and (4-6), deviation from the desired trajectory for a generalized coordinate can have an impact on the corresponding generalized force of other variables based on the values of $\mathrm{m_{ij}}$,$\mathrm{b_{ij}}$, and $\mathrm{k_{ij}}$. By assuming all non-diagonal elements of the coefficient matrices are zero, the generalized forces are assigned based on the deviation of corresponding generalized coordinates.

4.2 Implementation of Impedance Control on Cable Robots

An impedance controller allows deviations of the coordinates by applying some prescribed forces. Based on the assigned forces, the system acts as a mass-spring-damper. The impedance of the system can be indicated using the coefficients introduced in the previous section.

In rehabilitation procedures, it happens that the patient needs to deviate from the trajectory because of pain or because following the same trajectory is not applicable for the patient. However, the therapist wants the patient's limb to be forced to the original path.

Therefore, by choosing appropriate values of coefficients, the mechanism would be able to take the patient's arm along the desired trajectory and let him/her avoid excess pain.

Before implementing the impedance control on cable-driven mechanisms, the associated challenges which arise due to the cable tension condition needs to be addressed. As was explained in chapter 2, the equilibrium condition in a cable-driven system is expressed as:

$$\mathbf{At} = \mathbf{b} \tag{4-7}$$

where $\mathbf{t}$ is the vector of cable forces and $\mathbf{b}$ is the total value of other forces in the system (such as inertia, weight, etc.). $\mathbf{A}$ is a matrix of coefficients from the equilibrium equations. As was stated in chapter 1, the above equation can be derived using both Newton's and Lagrange's methods, but the obtained equations can be formed as equation (4-7) either way. For a multi-body mechanism, it is easier to develop the equations using Lagrange's methods and take the degrees of freedom as Lagrange's variables. In doing so, the following equation would be obtained.

$$\mathbf{A}_L\boldsymbol{\tau}_L = \mathbf{b}_L \tag{4-8}$$

where L subscript refers to the Lagrange's method. Also, it was said previously that the tensionability of the mechanism in a specific position depends on matrix $\mathbf{A}_L$. Moreover, all elements of matrix $\mathbf{A}_L$ are in terms of the generalized coordinates, q_i.

To implement impedance controller on a cable-driven mechanism, the patient who interacts with the robot should feel that the end-effector acts as a mass-spring-damper system. Therefore, a force other than weight and inertia forces of the bodies should be considered that represents the interacting force between the robot and the patient. That extra force is included as

$$\mathbf{b}_L = \mathbf{h}(q, \ddot{q}) + \mathbf{f} \tag{4-9}$$

where $\mathbf{f}$ is the interacting force between end-effector and the user. Also, $\mathbf{h}(q, \ddot{q})$ is a vector representing weight and inertia forces.

The solution for equation (4-8) is presented as:

$$\boldsymbol{\tau}_L = (\mathbf{A}_L{}^{\mathrm{t}}\mathbf{A}_L)^{-1}\mathbf{A}_L{}^{\mathrm{t}}[\mathbf{h}(q, \ddot{q}) + \mathbf{f}] + \alpha\mathbf{n} \tag{4-10}$$

where $\mathbf{n}$ is null vector of $\mathbf{A}_L$ and α is an arbitrary value.

Note that force $\mathbf{f}$ implies the impedance behavior of the mass-spring-damper. Therefore, it can be described as shown below.

$$\mathbf{f} = \mathbf{M}_L(\ddot{q_d} - \ddot{q}) + \mathbf{B}_L(\ddot{q}_d - \dot{q}) + \mathbf{K}_L(q_d - q) \tag{4-11}$$

where $\mathbf{M}_L$, $\mathbf{B}_L$ and $\mathbf{K}_L$ are the coefficient matrices, q_d is the desired position of mechanism in terms of Lagrange's coordinates

By deviating from the desired trajectory, the mechanism will apply a force to the patient based on equation (4-11).

The controller receives the measured positions of the generalized coordinates and calculates the interacting force using equation (4-11) and finds the required cable forces. Equation (4-10) returns the cable forces that make the end-effector apply force $\mathbf{f}$ on the environment. It is obvious that the calculated interacting force $\mathbf{f}$ by the controller is not essentially equal to the force $\bar{\mathbf{f}}$ that the user is applying.

From equation (4-10) one can find the cable tensile forces. The problem is that the coordinates of the patient's limb are very difficult to be directly measured. The only position that is measurable is the displacement of the cables from their initial position. This is completely doable by measuring the rotation angle of actuator's spool from its initial angle. By using forward kinematics one can find the length of cables in terms of the joint variables; but the inverse problem becomes more complicated in this type of robot. Because the length of each cable is a nonlinear and coupled function of joint variables:

$$\mathbf{l}_{1\times(n_{DoF}+1)} = \mathbf{g}(q_1, \dots, q_i, \dots, q_{n_{DoF}}) \tag{4-12}$$

where $\mathbf{l}$ is the vector of the cable lengths and $\mathbf{g}$ is a nonlinear function of joint variables.

Therefore, the position of the arm cannot be obtained in explicit form from the rotation angle of the motor spool.

The values of the joint variables are found by solving a set of nonlinear equations. Using the Newton-Raphson method, one can solve equation (4-12). Since there are $n_{DoF} + 1$ equations, one of the equations is redundant and can be omitted.

From measurement of joint variables, it is possible to determine the values of cable forces. The last step is assigning a value to α according to the equation (4-10). It was said in chapter 3 that a criterion for tensionability of a multi-body cable-driven system is to have all components of vector $\mathbf{n}$ of the same sign. Thus, by assigning an appropriate value for α, components of $\boldsymbol{\tau}_L$ become positive i.e. the system is tensionable.

The following algorithm was used in this study to assign a value to α. Since each cable has to be pulled with a minimum force to be straight enough and not slack, the algorithm returns α so that none of the cables will have a force less than that minimum value. In some cases this minimum value can be zero, if the weight of the cable is neglected. This problem can be divided into two cases.

The first one is when all the components of $\mathbf{n}$ are positive. In this case, the following equation was used to determine the value of α.

$$\alpha = max\ \{\frac{T_{min_i} - b_i}{n_i}\} \tag{4-13}$$

where T_{min_i} is the minimum value of tensile force for i^{th} cable, b_i is the i^{th} component of vector $\mathbf{b}_L$, and n_i is the i^{th} entry of $\mathbf{n}$.

The second case is when all the components of $\mathbf{n}$ are negative. The equation below shows how the value of α should be determined

$$\alpha = min\ \{\frac{T_{min_i} - b_i}{n_i}\} \tag{4-14}$$

Figure 4-3 shows the control process that executes in each cycle.

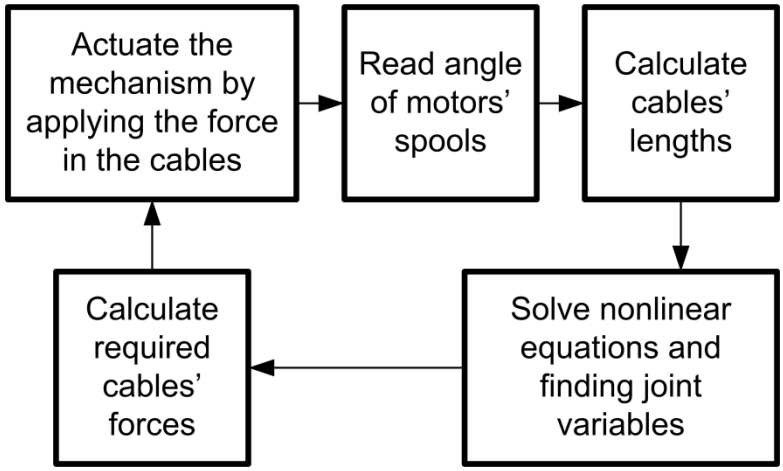

Figure 4-3 – Workflow of the controller

The control cycle first reads the encoder values and finds the angle of rotation then calculates the length of cables using the following formula:

$$l_i = R\gamma_i + l_{0_i} \tag{4-15}$$

where l_i is the length of the i^{th} cable and γ_i is the rotation angle of the i^{th} motor's spool. Also, l_{0_i} represents the initial length of the i^{th}cable . R is the radius of the motor's spool.

After obtaining the length of each cable, the control cycle solves (4-12) using Newton-Raphson method and finds joint variables that correspond to the position of the end-effector. By having the joint variables and the geometry of the system, the control cycle determines the required cable forces using equation (4-10) and actuates the motors by the obtained forces. For each new cycle, the controller goes through the described procedure again.

4.3 Modeling

In this section, implementation of an impedance controller on a rehabilitation cable robot is simulated using MATLAB SimuLink. The robot connects to and moves a shoulder.

A simplified model for the shoulder is assumed in this study. The figure below shows the assumed shoulder model.

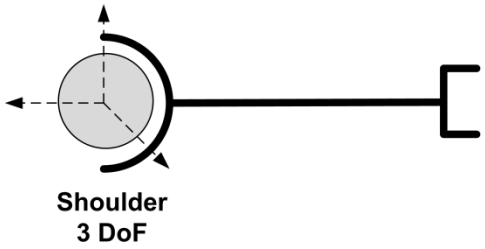

Figure 4-4 – Model of shoulder and arm

As shown in the figure above, the shoulder has been modeled with a spherical joint which rotates about three perpendicular axes. Therefore, the model has three degrees of freedom. The figure below shows how the arm model is placed in the robot.

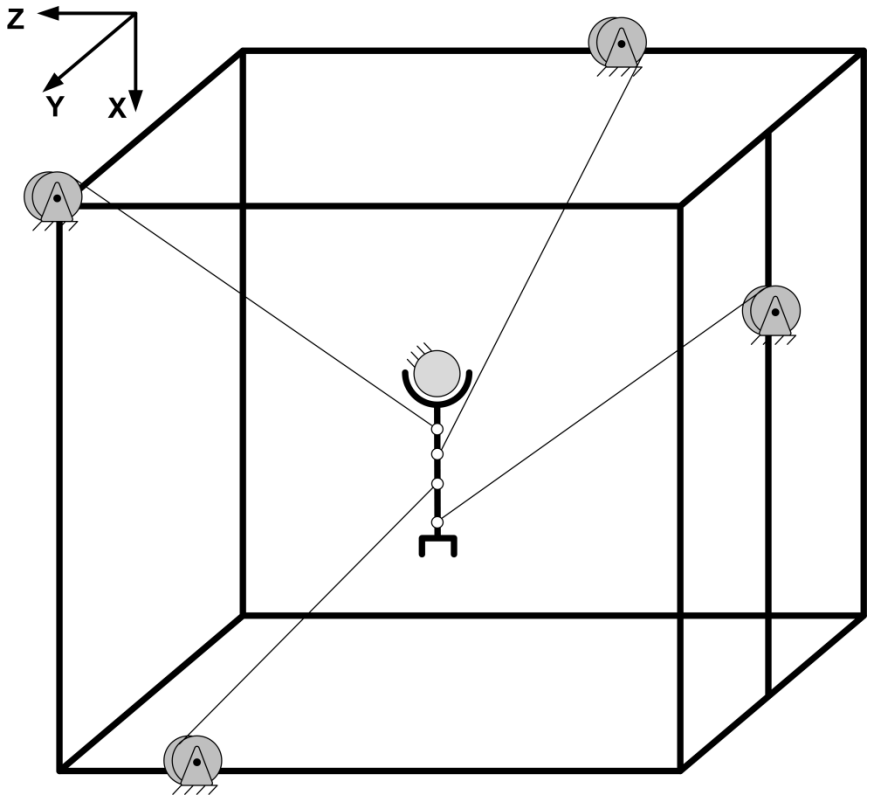

Figure 4-5 – Shoulder rehabilitation mechanism

As is shown in the figure above, there are 4 actuators assigned for this task, since the mechanism has 3 degrees of freedom. The center of the spherical joint was assumed as the origin of the fixed coordinate system

Lagrange coordinates are shown in an extended version of arm model in Figure 4-6.

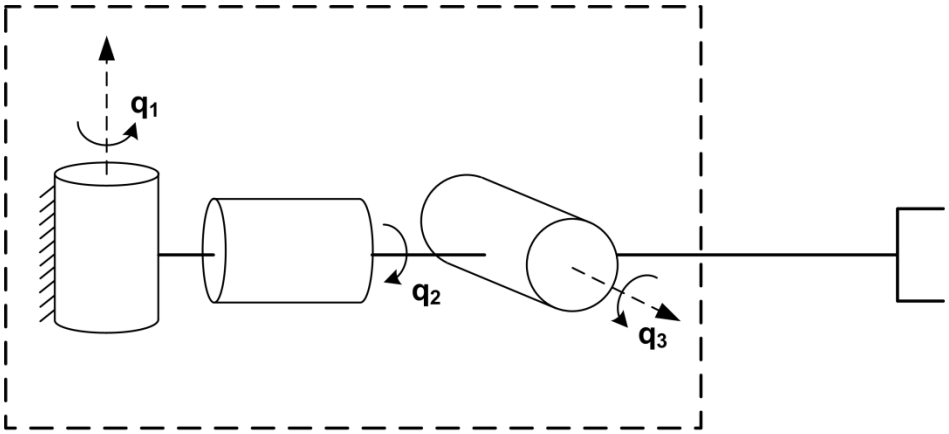

Figure 4-6 – Expanded model of shoulder joint

The desired workspace for the mentioned mechanism was assumed as shown in the table below.

Table 4-1 – Desired workspace of shoulder-arm model

	q_1	q_2	q_3
Minimum Value (rad)	-20	-20	0
Maximum Value (rad)	20	0	20

According to Chapter 02, we need to indicate a space for the design parameters. The design parameters in this problem are the positions of the actuators on the frame.

The same as introduce mechanism in chapter 3, one component of each actuator position is constant. Table 4-2 shows the Design Parameter Space of the robot and the constant components.

Table 4-2 – Actuators and their design parameters

Actuator	Plane	Fixed component	Design Parameters
1	Top	x	y_1, z_1
2	Back	y	x_2, z_2
3	Front	y	x_3, z_3
4	Right	z	x_4, y_4

According to Table 4-2, there are 8 design parameters. Table 4-3 shows the space including all the 8 design parameters.

Table 4-3 – Design Parameter Space

	y_1	z_1	x_2	z_2	x_3	z_3	x_4	y_4
Min. (mm)	-600	-600	-400	-600	-400	-600	-400	-600
Max. (mm)	600	0	400	100	400	100	1000	600

Also, the value of the fixed component for each actuator is listed in Table 4-4.

Table 4-4 – Constant component of each actuator

	Actuator 1	Actuator 2	Actuator 3	Actuator 4
Fixed Component Value (mm)	$x_1 = -596.0$	$y_2 = 1276.5$	$y_3 = -895.67$	$z_4 = -799.67$

The points where the cables are attached to the arm are expressed in cylindrical coordinates in Table 4-5. The cylindrical coordinate is a local coordinate system used to express the points with respect to the shoulder joint.

Table 4-5 – The points that attached to cables expressed in local cylindrical coordinate system

	$\mathbf{p_1}$	$\mathbf{p_2}$	$\mathbf{p_3}$	$\mathbf{p_4}$
Length l (mm)	275	240	251	254
Angleα (rad)	$-\frac{\pi}{2}$	$\frac{\pi}{2}$	$\frac{\pi}{3}$	$-\frac{\pi}{3}$

Kinematic synthesis for this mechanism was performed according to the method presented in Chapter 0. The step-sizes for workspace and Design Parameter Space were taken as $\left(\frac{q_{i_{max}}-q_{i_{min}}}{4}\right)$ and $20\ (cm)$ respectively.

Finally, the synthesis process returned the positions of the actuators listed in Table 4-6.

Table 4-6 – Position of actuators based on the mentioned global reference frame

Actuator Number	Position (mm)
1	[-595.60 -325.05 -1.17]
2	[389.85 -918.50 127.65]
3	[-481.92 895.67 111.55]
4	[-105.91 596.50 -799.67]

4.4 Modeling of the Actuators

The control approach in this thesis is about determining the required torque of each motor, because the motors are assumed to be working in torque control mode.

The actuator introduced in chapter 3 is modeled for the simulation in this section. Since the actuator is a type of brushless DC motor, the electrical dynamics were neglected in comparison with the mechanical dynamics of motor since dynamics of the electrical part is sufficiently fast compared with mechanical dynamics of the motor. To simplify the modeling, the transfer function of the actuators that explains the torque-position relation is considered as a linear transfer function [37]:

$$\frac{\theta(s)}{T(s)} = \frac{k}{Js^2 + Bs} \tag{4-16}$$

where J is the spool's moment of inertia, B is the damping coefficient. $\theta(s)$ is the rotation angle of motor and $T(s)$ is the total torque applied on the motor's shaft. Parameter k is a factor which depends on the dimension of J, B, and T. Figure 4-7 shows the model presented in equation (4-16).

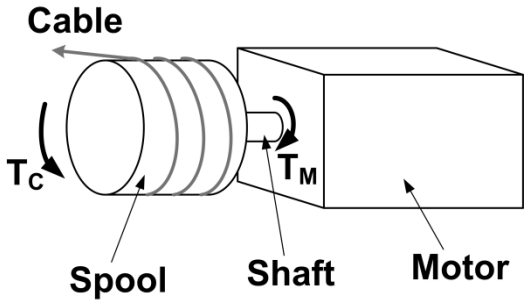

Figure 4-7 – Model of motor

In the figure above, two torques are applied on the motor's shaft. $T(s)$ is the sum of the motor's torque $T_M(s)$ and the cable's torque $T_C(s)$. In other words:

$$T(s) = T_M(s) - T_C(s). \tag{4-17}$$

Therefore, by having the cable's torque and electrical torque, one can find the angle of the motor's shaft. By multiplying equation (4-16) by the radius of the spool, the displacement in cable length is obtained.

$$\frac{\Delta l(s)}{T(s)} = \frac{R\theta(s)}{T(s)} = \frac{Rk}{Js^2 + Bs} \tag{4-18}$$

where Δl is the displacement in cable length. By considering gear ratio w, T_M will be multiplied by w. Therefore, the resultant output torque of the gear box will be wT_M.

In this study, the values of the parameters in equation (4-18) were assumed as following:

$$\frac{B}{J} = 10\left(\frac{N.s}{m^2.kg}\right); \frac{Rk}{J} = 161\left(\frac{s}{m^3.kg}\right) \tag{4-19}$$

Now, one can rewrite equation (4-16) in the following form.

$$\frac{\Delta l(s)}{T(s)} = \frac{161}{s^2 + 10s} \tag{4-20}$$

4.5 Simulation

According to Figure 4-7, one needs to have both T_M and T_C for simulation. The value of T_M is supposed to be assigned by the controller since the controller calculates the appropriate actuator force based on the algorithm shown in Figure 4-3.

Note that T_C is the torque that is applied by the cable and can be found using:

$$\boldsymbol{\tau}_L = (\mathbf{A}_L{}^{\mathrm{t}}\mathbf{A}_L)^{-1}\mathbf{A}_L{}^{\mathrm{t}}[\mathbf{h}(q, \ddot{q}) + T_O] + \alpha\mathbf{n} \tag{4-21}$$

where $\mathbf{h}(q, \ddot{q})$ includes all external forces applied on the arm except the cable forces such as weight and inertia. T_O is the generalized force applied by the patient. It was assumed that the arm moves with constant and very low velocity, and so the inertia forces were neglected. This assumption was made due to relatively slow motions in rehabilitation. In other words, rapid motions and high velocity tasks are not desired in physiotherapy. Therefore, neglecting inertia forces does not adversely affect the final results.

A MATLAB SimuLink model was developed as shown in Figure 4-8.

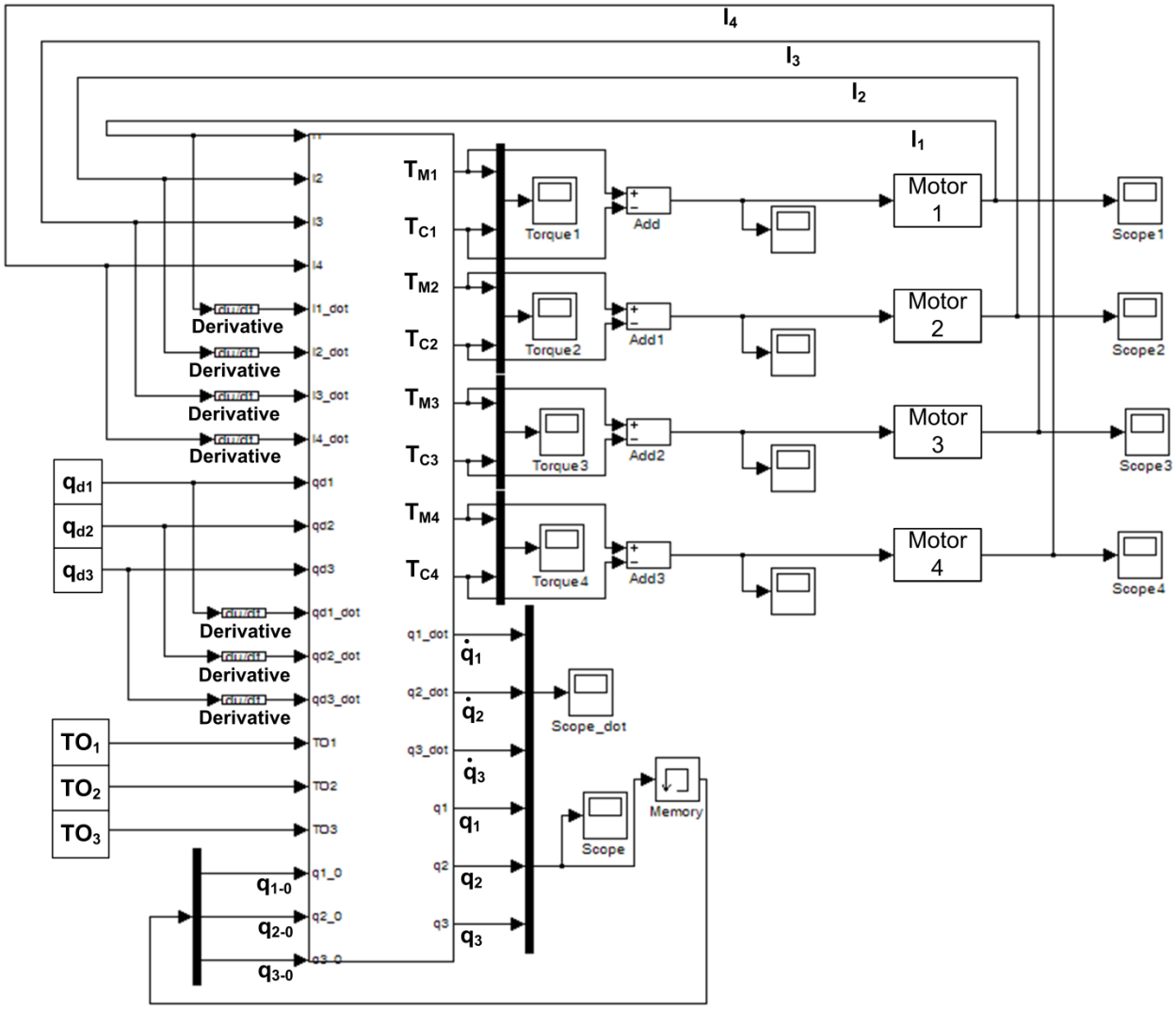

Figure 4-8 – MALTAB SimuLink Model

A core function was built that calculates the values of T_M and T_C. The transfer function of each motor returns the length of cable according to equation (4-20).

The core function takes the length of each cable and its derivatives based on the procedure above then determines the joint variables by solving equation (4-10) using the Newton-Raphson method. The code takes the previous values of joint variables as the initial guess and applies the iterative method of Newton-Raphson to find the values of q_{i-0}.

Having the desired values of joint variables (desired trajectory) as q_{d_i}, the code is able to calculate the impedance forces as T_{M_i}. The code is supposed to calculate T_{C_i} as the modeled forces of the cables applied on the motor spools. T_{O_i} are those external forces that are applied by the user (patient). T_{O_i} are considered as inputs to the model. One goal in this study is to model the patient's interacting force as input and check the functionality of the implemented method.

4.6 Results and Discussion

The coefficient matrices of impedance control were assumed as shown below as the desired values.

$$K = \begin{bmatrix} 4 & 0 & 0 \\ 0 & 3 & 0 \\ 0 & 0 & 1 \end{bmatrix};\ B = \begin{bmatrix} 1 & 0 & 0 \\ 0 & 0.5 & 0 \\ 0 & 0 & 0.3 \end{bmatrix} \tag{4-22}$$

The inertia matrix was neglected due to low acceleration and velocities.

In the first simulation, it was assumed that the arm is supposed to stay at an initial position ($q_{d_i} = 0$) in other words, the robot applies no motion to the arm. The patient applies an external force of $T_{O_1}, T_{O_2}, T_{O_3} = 0.1\sin(\frac{\pi}{40}t)$.

Figure 4-9 shows the joint variables vs. time.

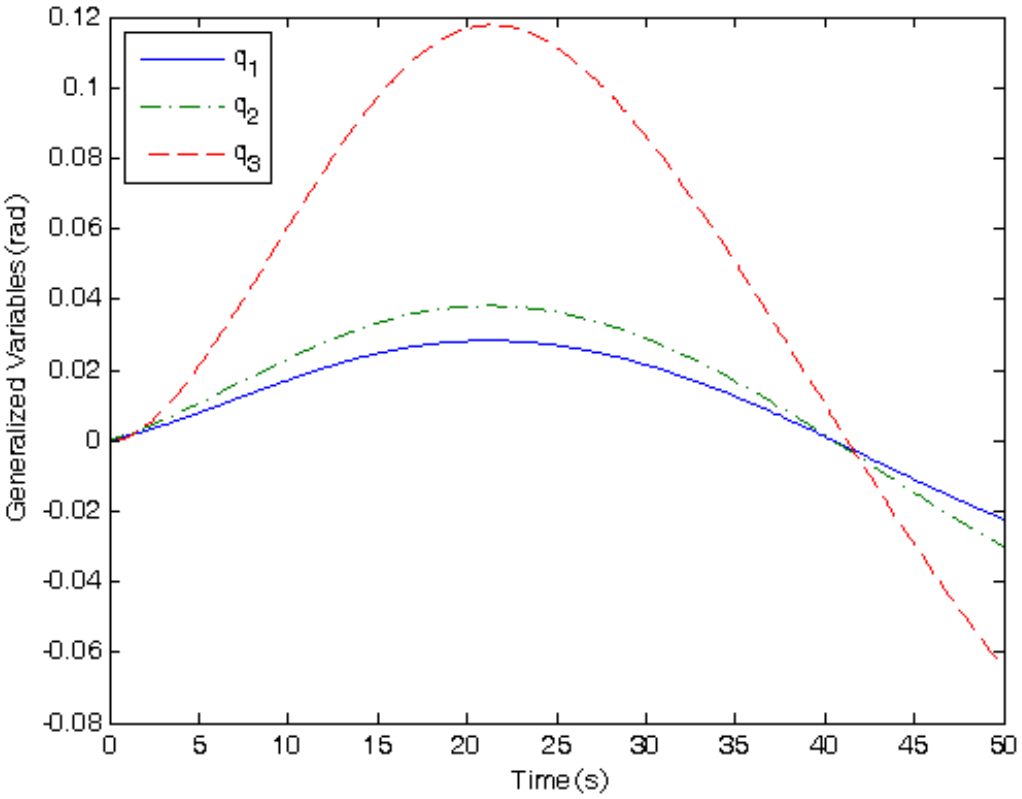

Figure 4-9 - Values of joint variables (rad) versus time (sec)

It is shown that the outputs are close to zero, which is the desired trajectory, but have a sinusoidal response. The sinusoidal response is due to having a sinusoidal patient's force.

Figure 4-10 shows the response of the three spring-damper systems with the same coefficients to the mentioned input (force).

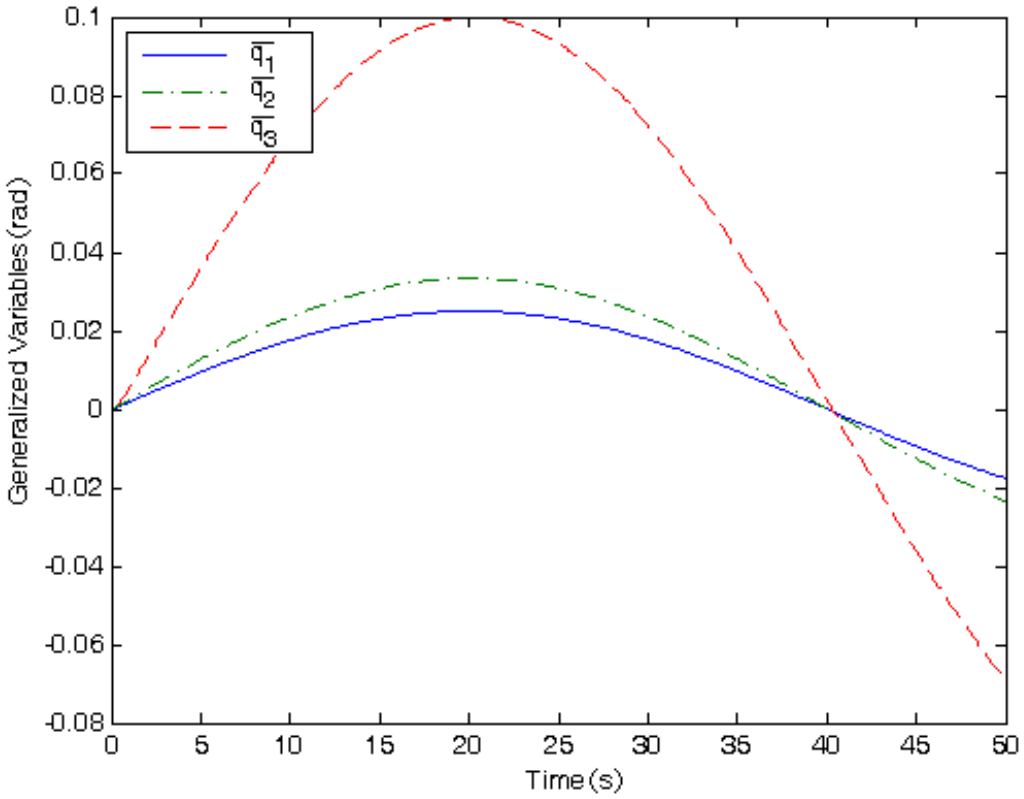

Figure 4-10 – Response of an ideal spring-damper system to the input force

In the figure above, $\bar{q}_i$ is the ideal value of i^{th} generalized variable. The ideal value is obtained by applying the same patient's force on the mass-spring-damper system.

Comparing Figure 4-9 with Figure 4-10, the output of the model is similar to the desired response of a spring-damper system, however some differences also can be seen. One difference is the initial slopes of the graphs. The actual output has a transient part initially and then starts rising, but the ideal response does not have it. Since the transfer function of motor shaft was taken into account in modeling, the output has a transient part and it involves a different initial slope. The ideal response is the value of the position based on governing equation of a mass-spring-damper system.

The other difference is on the peak values of the graphs where the outputs of the impedance control have higher peak values than the ideal responses. The existence of the overshoot is due to dynamics of the motor shaft. In other words, the dynamic of the shaft causes the actual values to pass the ideal values and then settle down.

The next step is to find the values of the spring and damper coefficients that the patient feels in this case. The simulation was used for parameter identification using the least-squares method to find the best fitted values for the damping and stiffness coefficients.

For a spring-damper system the equation below holds between the force and the position:

$$b\dot{x} + kx = f \tag{4-23}$$

where x is the position and b and k are the damper and spring coefficients, respectively. Also, f is the force applied on the system.

By having a sequence of positions and corresponding forces, one can write the equation as shown below:

$$b\dot{x}_i + kx_i = f_i \; ; i = 1,2, \dots, n \tag{4-24}$$

The derivative part can be written as shown below:

$$\dot{x}_i = \frac{x_{i+1} - x_i}{t_{i+1} - t_i} \tag{4-25}$$

where t_i is the corresponding time for position x_i.

One can also form equation (4-24) for all the values in the matrix format:

$$b\dot{\mathbf{x}} + k\mathbf{x} = \mathbf{f} \tag{4-26}$$

$$[\,\dot{\mathbf{x}} \quad \mathbf{x}]_{n\times 2} \begin{bmatrix} b \\ k \end{bmatrix}_{2\times 1} = \mathbf{f}_{n\times 1} \tag{4-27}$$

Where $\mathbf{x}$, $\dot{\mathbf{x}}$, and $\mathbf{f}$ are vectors of positions, velocities, and forces respectively.

Having equation (4-27), one can find the values of b and k based on the least-squares method, using the equations below.

$$\begin{bmatrix} b \\ k \end{bmatrix} = (\mathbf{y}^t\mathbf{y})^{-1}\mathbf{y}^t\mathbf{f} \tag{4-28}$$

$$\mathbf{y} = [\,\dot{\mathbf{x}} \quad \mathbf{x}] \tag{4-29}$$

Equation (4-25) does not return the exact derivatives and only calculates it numerically.

According to the presented method of estimation, the values of the coefficients obtained from the simulation outputs (Figure 4-9) are shown in Table 4-7 and compared to the desired values of controller coefficients.

Table 4-7 – Values obtained from simulation output using the Least-Squares method

	b_1	k_1	b_2	k_1	b_3	k_1
Desired	1	4	0.5	3	0.3	1
Least Square	3.24	3.37	2.35	2.39	0.69	0.88

As shown in the above table, the values of k are close to the desired ones, but the differences between the desired damping coefficients and the actual ones are significant. One reason is the existence of the transient part, due to considering dynamics of the motor shaft. Another reason is the natural error in controlling of systems that involve dynamics. In other words, every controlling scheme has error in the outputs due to the dynamics if the controlled system.

Also, as was previously stated, the nature of least-squares method involves error and it caused the obtained values to deviate more from the desired ones. To verify the previous sentence, a spring-damper system was simulated by applying a sinusoidal force of $f = 0.1sin(\frac{\pi}{40}t)\ N$. Figure 4-11 depicts the simulated spring-damper system as well as the applied force.

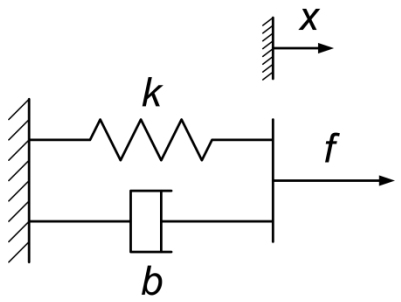

Figure 4-11 – Simulated spring-damper system

The measured position is shown below. The damping and stiffness coefficients are assumed to be 0.2 and 1 respectively.

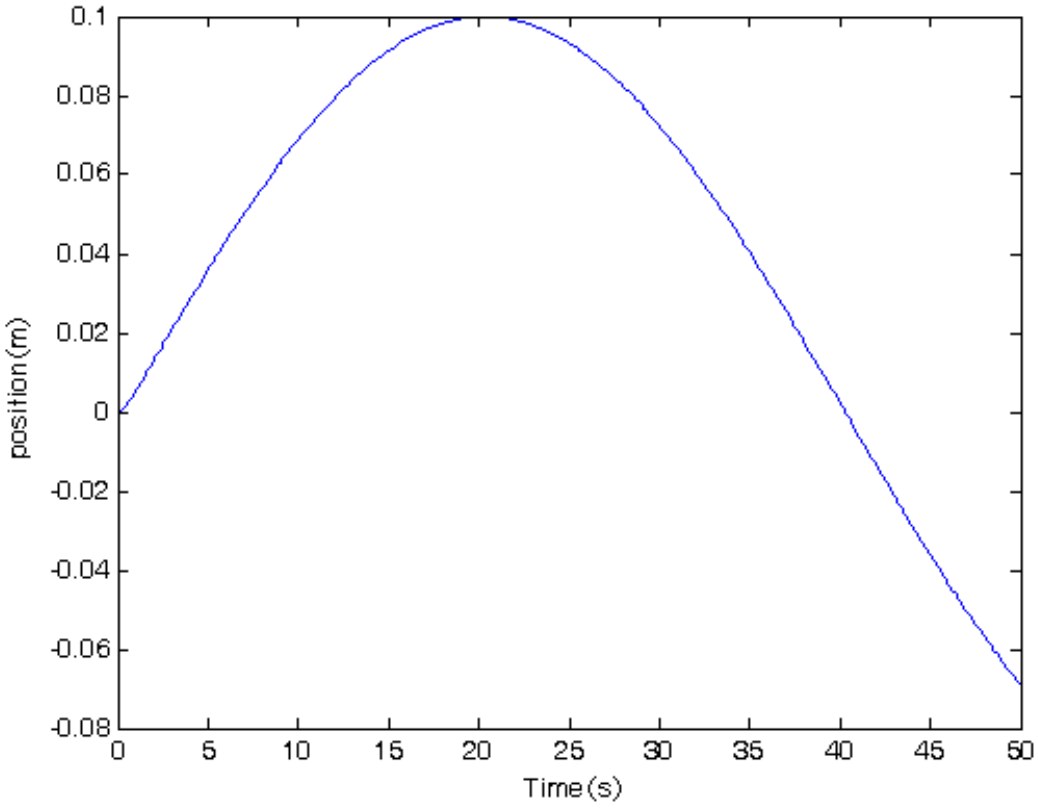

Figure 4-12 – Response of spring-damper system to a sinusoidal force input

The least square method applied to the measured data and the results were $b = 0.11789$ and $k = 1.00015$.

As was shown in the paragraph above, the obtained k from the Least Square method is close to the desired value, but the damping coefficient shows a significant difference between the desired value and the obtained one. The difference is possibly due to the approximation of the derivatives value using equation (4-25).

5 Conclusions and Recommendations for Future Work

5.1 Discussion

Design, calibration and operation of a cable-driven robot were investigated in this study as a new robotic platform for physical therapy. The mechanism is supposed to learn a motion from a therapist and redo it a specified number of times under controllable conditions.

Since rehabilitative motions are complex, they need complex mechanisms or several cooperative robots. The proposed mechanism had to be able to do complex tasks. Cable mechanisms are able to do high degrees of freedom motions using as many cable actuators as required. Using light cables compared to rigid links in conventional robotic mechanisms has enabled the robot to consume less energy and be cost-effective.

Moreover, since such a robot has to comply with the geometry and kinematics of different body parts in different sizes, the chosen mechanism must be reconfigurable and flexible in design. One advantage of the proposed cable mechanisms is that it is easily reconfigurable by changing the position of the actuators.

According to the above, a cable-driven mechanism was considered for synthesis, parameter identification and control of a rehabilitation robot. The upcoming paragraphs describe how each part was approached.

In the “Synthesis Chapter,” a methodology for design of the proposed rehabilitation robot was presented. The developed method finds parameters of the robot such that it covers the given workspace. An algorithm that does the synthesis process was developed.

The algorithm returns all configurations of a cable mechanism that is tensionable in a given workspace. In order to do so, the algorithm evaluates tensionability of a specific configuration for a desired workspace. By meshing the workspace, the algorithm checks the tensionability of each grid-point of workspace to ensure that the mechanism is tensionable for all the points within the workspace. Again, by meshing the parameter space and evaluating the desired workspace for each set of parameters, the configurations that make the robot tensionable for the given workspace were found.

Also, to optimize the synthesis results and pick the best configuration, an index function was introduced. The index value is a variance of cable forces during the operation. If the value is relatively small, it means forces of the cables are close together which is practically easier to realize and control. The optimization algorithm first finds the set of parameters that have the lowest value of the introduced index. Then it moves along the gradient of the mentioned index and determines the point that has the minimum index. Using this method, it prevents it from being trapped in the local minima.

The presented results at the end of the chapter verified the functionality of the proposed synthesis method. The proposed algorithm to synthesize and optimize the design was implemented on a 4 DoF rehabilitation cable robot.

A systematic approach for kinematic parameter identification of the proposed mechanism was also introduced. Since, the proposed robot needs to be reconfigured due to its application, the calibration should be achievable at low cost and in short time. The advantage of the presented method is that there is no need of extra equipment for the process. In other words, all the steps are done using the integrated encoders of the robot.

The presented method is based on the position of some known points and solving a set of nonlinear equations. The user takes the free end of the cable from one known point to another and records the difference between the initial and the final length of the cable. Based on the derived equations and the kinematic model of the actuator, the user is able to find the actual position of the motor. The equation is solved using the Newton-Raphson method.

The main challenges in the parameter identification were found to be the complexity of the geometry and model of the actuator. Since the cable is wound around the pulley installed on the cable guide assembly, the geometry of the cable was divided into two sections. One section was between the tangent point of the cable on the pulley and the known point. The other section was the curved part of the cable that lies on the pulley. Coupling the equations of these two sections, the tangent point was introduced as an auxiliary point. The final set of equations included the real position of the actuator and the tangent point as known variables.

At the end of identification chapter, the accuracy of the results was verified using a Faro arm and it was shown that the error of calculations was negligible compared to the size of the robot. It was shown that the introduced method of self-identification involves a maximum of 1.12 mm.

Finally a controller was developed for the proposed robot and evaluated by simulation in the last chapter. The goal of this chapter was to develop a controller that makes the rehabilitative motion pain-free to the patient. According to the Impedance Control theorem, position of end-effector is controlled by assigning an appropriate value of input force, such that the performance of the mechanism represents the impedance of a mass-spring-damper system. One of the main challenges was how to implement the Impedance Control Concept while maintaining positive tension in all cables.

Also, it was found that the values of the joint coordinates are not available since there is no sensor in the joints of the patient's body. Therefore, one needs to estimate them using forward kinematic equations. Since the equations were nonlinear, it was said that in each control cycle, the controller needs to solve the forward kinematics equations numerically and find the values of the joint coordinates.

In order to evaluate the controller, a cable mechanism and a shoulder model were were simulated using MATLAB SimuLink. The mechanism had 3 degrees of freedom and 4 actuators were considered, to ensure tensionability of the mechanism. Furthermore, the mechanism was assumed to have quasistatic motion due to the nature of rehabilitation. Therefore, the accelerations were neglected in the governing equations and the controller.

The simulation model was tested versus a mass-spring-damper. The results showed a general agreement however, some difference could be noted.The differences are listed below:

- The simulation has transient part initially.
- The peak values of measured data were greater than the response of a spring-damper system.
- A phase delay existed in the measured values of generalized coordinates.

The major reason for the above-mentioned difference is assumed dynamics for the motor's shaft. Since the shaft's transfer function had been taken into account in the modeling part, the system's outputs involved dynamics. The mentioned dynamics caused the over shoot and initial zero slope.

Also, the damping and stiffness coefficients were calculated using the Least Square method The other reason of existing difference is due to using the Least Square method which has a common error in estimation. The error of the Least Square method was shown using a simple spring-damper system. The results showed that the stiffness was close to the desired one, but the damping coefficient had a significant difference.

5.2 Future Work

Based on the acceptable results on the controller test in simulations, the immediate next step will be to test the controller on the real robot. Solving the nonlinear equations of the forward kinematics in real-time will be the main challenge of this step. Also, considering the displacement of the patient's shoulder in the controller can be another future work. In real practice the shoulder may involve displacement and the controller should be able to compensate that effect.

Investigation of effects of the non-diagonal elements of impedance control coefficients on the robot performance is another suggestion for the future work.

The mechanism that was synthesized and fabricated had 4 degrees of freedom and included shoulder and elbow joints. A wrist joint needs to be added in order to make it a realistic model of the human arm. The mechanism will have 7 degrees of freedom since the wrist adds 3 more degrees of freedom to the system. In that case, 8 actuators are needed to fulfill the tensionability requirement. Also, considering other limb of a human can be the following steps

for a rehabilitation robot. For instance, considering rehabilitation of a foot will bring in more points and issues that should be considered. This can be done by increasing the number of the cables so the robot will be able to handle a motion with more degrees of freedom.

Another suggestion for the future works is redoing the synthesis of the mechanism using Interval Analysis [20] and comparison of the results with the method presented here.

6 References

[1] Albus, J., Bostelman, R., and Dagalakis, N., 1993, "The NIST ROBOCRANE", *Journal of Robotic Systems,* **10**(5), pp. 709-724.

[2] Kawamura, S., and Ito, K., 1993, "A New Type pf Master Robot for Teleoperation Using a Radial Wire Drive System", *Proceedings of the IEEE/RSJ International Conference on Intelegent Robots and Systems,* Yokohama, Japan, pp. 55-60.

[3] Dekker, R., Khajepour, A., and Behzadipour, S., 2006, "Design and Testing of an Ultra High-Speed Cable Robot", *Journal of Robotic and Automation,* **21**(1), pp. 25-34.

[4] Rezazadeh, S., and Behzadipour, S., 2007, "Tensionability Condistions of a Multi-Body System Driven by Cables", *Proceeding of ASME International Mechanical Engineering Congress and Exposition - IMECE,* Seattle, WA, USA.

[5] Verhoeven, R., and Hiller, M., 2000, "Estimating the Controllable Workspace of Tendon-Based Stewart Platforms", *Proceeding of 7th International Symposium on Advances in Robot Kinematics ARK,* Protoroz, Slovenia, pp. 277-284.

[6] Alp, A.B., and Agrawal, S.K., 2002, "Cable-Suspended Robots: Design Planning and Control", *Proceeding of IEEE conference on Robotics & Automation,* Washington, DC, USA.

[7] Pusey, J., Fattah, A., Agrawal, S., Messina, E., and Jacoff, A., 2003, "Design and Workspace Analysis of a 6-6 Cable-Suspended Parallel Robot", *Proceedings of IEEE International Conference on Intellegent Robots and Systems,* Las Vegas, NV, USA.

[8] Zi, B. and Zhu, Z.C., 2010, "Design and Analysis if Completely Restrained Cable Manipulators with 3 Degrees of Freedom", *Proceeding of the 8th World Congress on Intelligent Control and Automation*, Jinan, China.

[9] Gouttefarde, M., Gosselin, C. M.,2006, "Analysis of the wrench-closure workspace of planar parallel cable-driven mechanisms", *IEEE Transactions on Robotics*, Vol. 22, issue 3, pp. 434–445.

[10] Chen, Q., Chen, W., Liu, R., and Zhang, J., 2009, "Structure Optimization and Tension Analysis of a Cable-Driven Spherical Joint", *IEEE International Conference on Control and Automation*, New Zealand.

[11] Hassan, M., Khajepour, A., 2009, "Analysis of a Large-Workspace Cable-Actuated Manipulator for Warehousing Applications", *Proceeding of the ASME 2009 Intenational Desing Engineering Technical Conferences & Computers and Information in Engineering Conference*, San Diego, California, USA.

[12] Alikhani, A. , *Behzadipour*, S.,; Sadough Vanini, S.A., Alasty, A., 2009, "Workspace Analysis of a Three DOF Cable-Driven Mechanism", *Journal of Mechanisms and Robotics*, v 1, n 4, pp. 1-7.

[13] Alikhani, A. , *Behzadipour*, S.,; Sadough Vanini, S.A., Alasty, A., 2011, "Design of a large-scale cable-driven robot with translational motion", *Robotics and Computer-Integrated Manufacturing*, **27**, pp. 357-366.

[14] Oftadeh, R., Aref, M.M., and Taghirad, D.H, 2010, "Forward Kinematics Analysis of A Planar Cable Driven Redundant Parallel Manipulator Using Force Sensors", *Proceeding of IEEE/RSJ International Robots and Systems*, Taipei, Taiwan.

[15] Du, J., Bao, H., Duan, X., and Cui, C., 2010, "Jacobian Analysis of a long-span cable-driven manipulator and its application to forward solution", *Mechanism and Machine Theory*, **45**, pp. 1227-1238.

[16] Pham, C.B., Yeo, S.H., Yang, G., Chen, I.-M., 2009, "Workspace Analysis of Fully Restrained Cable-Driven Manipulators", *Robotics and Autonomous Systems*, **57**, pp. 901-912

[17] Zhang, Y., Zhang, Y., Xiaowei, D., Yang, Y., 2009, "Workspace Analysis of a novel 6-dof cable-driven parallel robot", Proceeding of IEEE *International Conference on Robotics and Biomimetics*, Guilin, China.

[18] Lim, W.B., Yang, G., Yeo, S.H., Mustafa, S.K., and Chen, I.-M., 2009, "A Generic Tension-Closure Analysis Method for Fully-Constrained Cable-Driven Parallel Manipulators", *Proceeding of IEEE International Conference on Robotics and Automation*, Kobe, Japan.

[19] Hernández-Martínez, E. E., Ceccarelli, M., Carbone, G., López-Cajún, C.S. and Jáuregui-Correa, J.C., 2010, "Characterization of a Cable-Based Parallel Mechanism for Measurement Purposes", *Mechanics Based Design of Structures and Machines*, 38(1), pp. 25-49

[20] Gouttefarde, M., Merlet, J-P., and Daney, D., 2007, "Wrench-Feasible Workspace of Parallel Cable-Driven Mechanisms", *Proceeding of IEEE International conference on Robotics & Automation,* Roma, Italy.

[21] Gouttefarde, M., 2008, "Characterizations of fully constrained poses of parallel cable-driven robots: A Review", *Proceeding of the ASME 2008 International Desig Engineering Technical Conferences & Computers and Information in Engineering Conference*, Brooklyn, New York, USA.

[22] Loloei, A.Z., Aref, M.M., Taghirad, H.D., 2009, "Wren Feasible Workspace Analysis of Cable-Driven Parallel Manipulators Using LMI Approach", *IEEE/ASME International Conference on Advanced Intelligent Mechatronics*, Singapore.

[23] Castelli, G., Ottaviano, E., Gonzalez, A., 2010, "Analysis and Simulation of a new Cartesian Cable-Suspended Robot", *Proceeding of the Intituion of Mechanical Engineers, Part C: Journal of Mechanical Engineering Science*, **224**, pp. 1717-1726

[24] Bouchard, S., Gosselin, C., Moore, B., 2010, "On the Ability of a Cable-Driven Robot to Generate a Prescribed Set of Wrenches", *Journal of Mechanisms and Robotics*, v 2, n 1, pp. 1-10.

[25] Rezazadeh, S., and Behzadipour, S., 2011, "Workspace Analysis of Multibody Cable-Driven Mechanisms", *Journal of Mechanisms and Robotics*, **3**(2), pp. 0210052(1-10).

[26] Fattah, A., and Agrawal, S.K., 2005, "On the Design of Cable-Suspended Planar Parallel Robots", *ASME Journal of Mechanical Design,* **127**(5), pp. 1021-1028.

[27] Merlet, J-P, 2005, "Opyimal design of robots, in Proc. Robotics: Science and Systems", Cambridge, MA USA.

[28] Gouttefarde, M., Krut, S., Company, O., and Pierrot., F., and Ramadani, N., 2008, "On the Design of Fully Constrained Parlle Cable-Driven Robots", *ASME Journal of Advances in Robot Kinematics: Analysis and Design,* pp. 71-78.

[29] Xu, L., Cao, Y., Chen, J., and Jiang, S., 2010, "Design and Workspace Optimization of a 6/6 Cable-Suspended Parallel Robot", *Proceeding International Conference on Computer Application and System Modeling*, Taiyuan, China.

[30] Zanotto, D., Rosati, G., and Aldo, R., 2010, "Performance Analysis of Planar Cable-Based Parallel Manipulators", *Proceeding of the ASME 2010 Biennial Conference Engineering Systems Design and Analysis*, Istanbul, Turkey.

[31] Yao, R., Tang, X., Wang, J., and Huang, P., 2010, "Dimensional Optimization Design of the Four-Cable-Driven Parallel Manipulator in FAST", *IEEE/ASME Transaction on Mechatronics*, **15**(6), pp. 932-941

[32] Jihui, Z., Qingsong, C., and Dan, L., 2010, "Design of a Novel Cable-Driven Robot for Rehabilitation", *Proceeding of International Conference on Mechanic and Control Engineering*, Wuhan, China. *(MACE)*

[33] Ginsberg, J.H., 1998, "Advanced Engineering Dynamics", Second Edition, Cambridge University Press.

[34] http://www.faro.com/FaroIP/Files/File/Downloads/User%20Manuals/08M46E00%20-%20FaroArmUSB%20-%20January%202009.pdf, June 1st, 2011.

[35] http://products.faro.com/product-overview/, June 12, 2011.

[36] Kazerooni, H., 1987 "Robust, Non-Linear Impedance Control for Robot Manipulators" *IEEE International Conference on Robotics and Automation*, Raleigh, North Carolina, March.

[37] Franklin, G.F., Powell, J.D., Emami-Naeini, A., 2006, "Feedback Control of Dynamic Systems", Fifth Edition, Pearson Education, Inc..